Supramodal Shape Representation in the Human Brain

Yangwen Xu[1]*, Lorenzo Vignali[12], Federica Sigismondi[1], Davide Crepaldi[2], Roberto Bottini[1], Olivier Collignon[134]*

[1]Center for Mind/Brain Sciences (CIMeC), University of Trento, Trento, Italy

[2]International School for Advanced Studies (SISSA), Trieste, Italy

[3]Psychological Sciences Research Institute (IPSY) and Institute of NeuroScience (IoNS), University of Louvain, Louvain-la-Neuve, Belgium

[4]School of Health Sciences, HES-SO Valais-Wallis, The Sense Innovation and Research Center, Lausanne and Sion, Switzerland

* Corresponding authors

Abstract

We can sense an object's shape by vision or touch. Previous studies suggested that the inferolateral occipitotemporal cortex (ILOTC) implements supramodal shape representations as it responds more to seeing or touching objects than shapeless textures. However, such activation in the anterior portion of the ventral visual pathway could be due to the conceptual representation of an object or visual imagery triggered by touching an object. We addressed these possibilities by directly comparing shape and conceptual representations in early blind (who lack visual experience/imagery) and sighted participants. We found that bilateral ILOTC in both groups showed stronger activation during a shape verification task than during a conceptual verification task made on the names of the same manmade objects. Moreover, the distributed activity in the ILOTC encoded shape similarity but not conceptual association among objects. Besides the ILOTC, we also found shape representation in both groups' bilateral ventral premotor cortices and intraparietal sulcus, a frontoparietal circuit relating to object grasping and haptic processing. In contrast, the conceptual verification task activated both groups' left perisylvian brain network relating to language processing, and, interestingly, the cuneus in early blind participants only. The ILOTC had stronger functional connectivity to frontoparietal circuit than to the left perisylvian network, forming a modular structure specialized in shape representation. Our results conclusively support that the ILOTC selectively implements shape representation independently of visual experience, and this unique functionality likely comes from its privileged connection to the frontoparietal haptic circuit.

Introduction

Object properties can be accessed through multiple sensory channels. For instance, knowledge of an object's shape can be acquired both by vision and touch. This brings up a critical question about the cerebral architecture of object representation: Are shape representations derived from different senses segregated from each other in the human brain or, alternatively, could the brain implement a shared representation of object shape that is abstracted from the senses (e.g., Amedi et al., 2005; Lacey et al., 2009; Ricciardi et al., 2014; Bi et al., 2016)?

Cognitive neuroscientists usually investigate object shape representation along separate visual and haptic brain pathways. Studies on visual shape representation mostly focus on the ventral visual pathway in the occipitotemporal cortex. Researchers found that the lateral occipital cortex and the posterior fusiform gyrus (i.e., the lateral occipital complex, LOC) show greater activation to object images than texture images (see review by Grill-Spector et al., 2001). By contrast, the medial part of the visual cortex is more sensitive to visual texture than visual shape (e.g., Peuskens et al., 2004; Cant & Goodale, 2007; Cant et al., 2009). Lesions in the LOC induce visual form agnosia manifested as impaired shape discrimination but preserved texture discrimination performance (Milner et al., 1991; James et al., 2003), whereas lesions in the medial part of the visual cortex cause the opposite syndrome (e.g., Cavina-Pratesi et al., 2010).

Studies on haptic shape representation highlighted the neural circuit in the ventral frontoparietal cortex. Researchers found that the intraparietal sulcus (IPS; e.g., Amedi et al., 2001, 2002; Stilla & Sathian, 2008; Snow et al., 2015) and the ventral part of the premotor cortex (vPMC, e.g., Stilla & Sathian, 2008; Snow et al., 2015) show greater activation when participants touch objects than textures. Lesions in the superior parietal cortex and the adjacent IPS induce contralateral tactile agnosia characterized

by somatosensory discrimination deficits in the macrogeometrical domain (i.e., detecting differences in length of cuboids) but not in the microgeometrical domain (i.e., detecting subtle differences in grating profiles), whereas lesions in the postcentral gyrus cause the opposite syndrome (Hömke et al., 2009). Lesions in the anterior IPS (aIPS) and vPMC can also impair contralateral object exploration—patients cannot recognize objects haptically due to the disturbance of finely tuned finger movements, specifically when interacting with objects (Binkofski et al., 2001; Dettmers et al., 2003). In the macaque brain, the homologous regions of both the aIPS (i.e., the AIP) and the vPMC (i.e., the F5) host the neurons that fire when monkeys configure their hands to grasp objects in particular shapes (e.g., Murata et al., 1997, 2000).

Research on visual and haptic shape representations intriguingly converge on the anterolateral part of the LOC in the inferolateral occipitotemporal cortex (ILOTC), a region that shows stronger activation when participants both see or touch objects in comparison to shapeless textures (e.g., Amedi et al., 2001, 2002; Stilla & Sathian, 2008; Snow et al., 2015). This region was therefore termed the lateral occipital tactile-visual complex (LOtv; Amedi et al. 2002) and is suggested to implement supramodal shape representation (Ricciardi et al., 2014). However, the nature of lLOTC remains debated as current findings could also support alternative hypotheses.

First, the LOTC might engage in haptic tasks simply due to visual imagery. This hypothesis is supported by studies showing that experiences of visual imagery during haptic shape perception are common and ratings of the vividness of visual imagery strongly predict the amount of haptic shape-selective activity in the right LOC (Zhang et al., 2004). To test whether visual imagery is a prerequisite for ILOTC's involvement during nonvisual tasks, two studies have tested early blind participants who lack visual imagery. These two studies, however, do not allow to settle the debate. One study found ILOTC's activation when contrasting a haptic object recognition task and a task imitating the grasping

and exploration of objects (Amedi et al., 2010). Since this study did not match the two contrasted conditions on task demand and object semantics (see next paragraph), the isolated cognitive components therefore might not be specific to shape processing. The other study, instead, did not find that the lLOTC encoded object shape in the early blind participants and localized shape representation in other occipitotemporal regions (Peelen et al., 2014). Participants in this study performed a shape-irrelevant task (i.e., size judgment task), which might have dampened the brain activation relating to shape representation in the lLOTC.

Second, the lLOTC might engage in conceptual representation of objects. An object does not only have a shape; it carries meaning and serves a function. Whenever in the above contrasts between objects and textures (e.g., Amedi et al. 2001, 2002) or between the haptic condition with objects and the hand-movement condition without objects (Amedi et al., 2010), the isolated cognitive component could be conceptual, not perceptual. Previous studies have shown that the ventral visual pathway can indeed encode semantic relatedness among objects (e.g., Carlson et al., 2014). This is even more likely for the lLOTC, a region showing category preference for manmade objects that cannot be fully explained by visual features (e.g., Bracci et al., 2016) and persists in the early blind participants (e.g., Pietrini et al., 2004; Peelen et al., 2013; Wang et al., 2015; Dormal et al., 2018; Mattioni et al., 2020). Further evidence has shown that patients with lesions in the left lateral occipitotemporal cortex, a region close to the lLOTC, are slower to make thematic associations among manmade objects (e.g., hammer-nail) (Kalénine and Buxbaum, 2016). However, this hypothesis was challenged by a recent study showing that the activity pattern in the lLOTC can encode object shape when stimuli are meaningless novel shape models (Lee Masson et al., 2016). Nevertheless, these findings cannot rule out lLOTC's involvement in conceptual representation; the lLOTC might support an integrative coding of both visual and conceptual knowledge, as already shown in some other regions in the ventral visual stream (Martin et al., 2018).

Third, the ILOTC might engage in (visual) shape representation in the sighted but conceptual representation in the early blind. Indeed, due to a lack of visual input since birth, the "visual" cortex in the early blind, accompanied by its enhanced connectivity to high-order brain systems, could repurpose its function for cognitive faculties distant from its native computation in vision, like language or mathematics (see Bedny, 2017 for review). In line with this idea, it has been reported that the lateral occipital cortex in the early blind, a region near the ILOTC, is more sensitive to semantic tasks (Noppeney et al., 2003) and lexical semantics (e.g., Bedny et al., 2011) than in the sighted participants. Moreover, the activity in the lateral occipital cortex in the early blind is more synchronized to the areas in the perisylvian language network than in the sighted participants (Bedny et al., 2011). It is thus possible that the ILOTC in the early blind implements conceptual instead of shape representation due to functional reorganization (Bedny, 2017).

To address these unsolved questions comprehensively in a single study, we used functional Magnetic Resonance Imaging (fMRI) to characterize the brain activity of sighted and early blind participants when they were performing both shape and conceptual verification tasks on the same set of auditory words referring to manmade objects. Importantly, we orthogonalized the pairwise shape similarity and the pairwise conceptual association among the objects we selected (e.g., a "plate" is perceptual similar to a "coin" in shape but is conceptually associated with a "fork" in function). Univariate and representational similarity analyses (RSA; Kriegeskorte et al., 2008) were conducted to localize and characterize the regions implementing shape and conceptual representation. Resting-state functional connectivity (RSFC) was used to detect possible synchronization between the ILOTC and the frontoparietal haptic network or the perisylvian language network.

If the ILOTC implemented supramodal shape representation, we would find the ILOTC showing greater activation in the shape task than in the conceptual task in both sighted and early blind participants, and the activity pattern in the ILOTC would encode objects' shape but not conceptual properties. The ILOTC would have stronger connections to the frontoparietal haptic network than the perisylvian language network. If the ILOTC represented objects' conceptual knowledge instead, we would observe greater activation in the conceptual task than in the shape task in both sighted and early blind participants, and the activity pattern in the ILOTC would encode objects' conceptual properties. Alternatively, if the activation in the ILOTC depended on visual experience, we would discover the ILOTC's involvement in shape processing/representation only in the sighted but not in the early blind participants. If such "visual" ILOTC repurposed its function to conceptual processing in the early blind, we could find the ILOTC's involvement in conceptual processing/representation only in the early blind but not in the sighted participants.

Results

Behavior rating on shape similarity and conceptual association

In this study, we selected 21 Italian words, which referred to 21 manmade objects, as our stimuli. The selection was mostly based on behavior ratings of object properties from an independent group of sighted participants who did not take part in the fMRI experiment (N = 19; see Stimuli in Materials and Methods about the stimulus selection procedure and criteria). To validate the rating results from the stimulus selection stage and to verify whether the early blind population had similar shape and conceptual knowledge as the sighted control, all participants who took part in the fMRI experiments (N = 48) also rated the object properties of the stimuli selected. These participants formed into three groups: 16 early blind (EB) participants, 16 gender- and age-matched sighted control (SC) participants, and 16 independent sighted (IS) participants (see Participants in Materials and Methods for details).

Shape similarity and conceptual association were rated on a 7-point Likert scale in a pairwise manner (see Procedures in Material and Methods about the rating procedure). We assessed the inter-rater reliability within each group of participants using the intraclass correlation based on a mean-rating, consistency, two-way random model (i.e., ICC(C,k)) (McGraw & Wong, 1996). Both shape rating (ICC(C,k): 0.953-0.973) and conceptual rating (ICC(C,k): 0.984-0.985) showed "excellent" inter-rater reliability (Koo & Li, 2016) (Supplementary Table 3). We averaged the rating scores within each group and compared them across groups. Figure 1A illustrates that the rating scores on both object properties were highly reliable across three groups (r(208) on shape similarity: 0.957-0.983; on conceptual association: 0.982-0.984), and the pairwise shape similarity was orthogonal to the pairwise conceptual association (r(208): 0.103-0.132).

We then averaged the pairwise rating scores of all the participants (N = 48) and calculated the representational dissimilarity matrix (RDM) of shape similarity and conceptual association (i.e., 7 minus the mean rating score). The resulting two Model RDMs had comparable variance across pairs of objects (shape similarity: variance = 2.163; conceptual association: variance = 2.498) and therefore offered equated discovery possibilities when correlated with brain RDMs in the subsequent representational similarity analysis. Figure 1B-C shows the organizational structure of the two RDMs, where 21 items were grouped according to the clusters generated by the k-means clustering algorithm (Lloyd, 1982; Vassilvitskii & Arthur, 2006), with the silhouette criterion used to decide the optimal number of clusters (Rousseeuw, 1987). The shape similarity RDM fell into three clusters, corresponding to square, round, and elongated objects (Figure 1B). The conceptual association RDM fell into seven smaller clusters, corresponding to different occasions in which objects were used (Figure 1C). For example, the two biggest clusters were related to eating and writing. The conceptual rating results accorded closely with the teleological perspective, which suggests the essence of a manmade object lies in its function, not its physical properties (e.g., Bloom, 1996).

Behavior rating on other object properties and confounding factors

Potential confounding factors were also considered. It has been reported that other properties of manmade objects can also modulate brain activity, like object size (big vs. small; e.g., Konkle & Oliva, 2012), toolness (tools vs. non-tool manmade objects; e.g., Chen et al., 2018), and contextual association (strong vs. weak contextual association objects; e.g., Bar & Aminoff, 2003). These three variables were rated on a 7-point Likert scale (see Procedures in Material and Methods about the rating procedure). Supplementary Table 3 shows the inter-rater reliability within each group of participants. The inter-rater reliability reached "excellent" on object size (ICC(C,k): 0.979-0.992) and varied from "good" to "excellent" on toolness (ICC(C,k): 0.893-0.928). The inter-rater reliability on contextual

association differed between sighted and early blind groups. While sighted groups had a "good" to "excellent" inter-rater reliability (SC: ICC(C,k) = 0.856; SI: ICC(C,k) = 0.919), the early blind group only had a "moderate" one (EB: ICC(C,k) = 0.613). Such heterogeneity in the early blind might result from a lack of instantaneous and global information about the environment from the visual input.

Besides the three object properties, all participants rated on a 7-point Likert scale about the degree to which they knew each objects' typical shape and primary function. Since most stimuli selected were everyday objects, both shape and conceptual rating scores hit the ceiling and varied only slightly across objects (averaged shape familiarity score across objects: M = 6.744, SD = 0.285; averaged conceptual familiarity score across objects: M = 6.944, SD = 0.066). Participants also rated how frequently they touched each object (1: have never touched it before; 7: touch it every day), which can be considered a sensitive and common index reflecting object familiarity across sighted and early blind groups. The inter-rater reliability on touch experience within each group of participants reached "excellent" (ICC(C,k): 0.965-0.975; Supplementary Table 3).

We averaged the above rating scores within each group of participants and evaluated the reliability of the mean rating score across participant groups. Figure 1B shows that the rating scores across three groups of participants were reliable (r(19) on objects size: 0.973-0.998; on contextual association: 0.732-0.940; on toolness: 0.883-0.933; on touch experience: 0.935-0.974). From this figure, we can also spot a moderate positive correlation between object size and contextual association (r(19): 0.363-0.529) and between toolness and contextual association (r(19): 0.264-0.622), which means the bigger the size and the more likely an object is a tool, the more likely this object is bound to a specific context. Moreover, we also added two linguistic measures—word frequency (i.e., the Zipf value of the word occurrence in film and television subtitles; http://crr.ugent.be/subtlex-it/) and word duration. There

was a moderate positive correlation between word frequency and touch experience (r(19): 0.419-0.446) and a moderate negative correlation between word frequency and word duration (r(19) = -0.577).

We then averaged the rating scores across all participants (N = 48) to get a mean rating score vector for each rating item. Figure 1E illustrates the Z-scores of all the ratings across objects. To orthogonalize these unidimensional variables, we conducted the principal component analysis and applied varimax rotation to improve the interpretability of the resulting principal components. Five components had eigenvalues greater than 1. Figure 1F shows the correlation of these five rotated components (RCs) with each rating item. RC1 to RC5 corresponded to object size, toolness, touch experience, word frequency, and word duration, respectively (r(19): 0.915-0.981). The RCs corresponding to object size and toolness also had moderate correlations with the contextual association (r(19): 0.656 and 0.584). These RC scores were used in the subsequent parametric modulation analysis.

Performance on shape and conceptual task during scanning

During the scanning, participants performed two tasks on the same set of auditorily presented words. In the shape verification task, participants thought carefully about the typical shape of each object and judged whether it was elongated, angular, hollow, circular, and disc-shaped. In the conceptual verification task, participants thought carefully about the primary function of each object and judged whether it was for eating, writing, sleeping, lighting, and purchasing (see Procedures in Materials and Methods for details).

Table 1 shows the accuracy and reaction time (RT) across participants within each group in shape and conceptual verification tasks. All groups of participants had near-ceiling accuracy on both tasks. The shape verification task took about 130-200 ms longer than the conceptual verification task. We built a

linear mixed model to predict the RT in the correct trials with groups of participants (EB vs. SC) and types of tasks (shape vs. conceptual tasks) as fixed effects variables and each participant as random effects grouping factors. The analysis revealed a significant task effect ($F(1,30) = 73.055$; $p < 0.001$), whereas neither the group effect ($F(1,30) = 0.732$, $p = 0.399$) nor the interaction effect between groups and tasks ($F(1,30) = 2.552$, $p = 0.123$) were found significant. Such difference between shape and conceptual tasks is in line with the evidence suggesting that retrieving specific semantic features (e.g., shape knowledge) requires more time than general semantic knowledge (e.g., Hauk, 2016).

Shape compared to conceptual tasks engaged ILOTC in both EB and SC.

We first contrasted the neural activity level between the shape and conceptual tasks. To remove the domain-general RT effect, we modeled the trial-by-trial RT variability across two tasks in the first-level general linear model using both the variable epoch approach and the variable impulse approach (Grinband et al., 2008). Figure 2 illustrates results while the domain-general RT effect was controlled (vertex-wise $p < 0.001$, cluster-level family-wise error (FWE) corrected $p < 0.05$).

Figure 2A shows the contrast of shape task vs. conceptual task using all participants ($N = 48$). The shape task and the conceptual task involved dissociable brain networks. The shape task activated bilateral brain areas, including the ILOTC (i.e., the lateral part of the Broadman area (BA) 37), the anterior IPS (aIPS), the posterior IPS (pIPS), the ventral part of the premotor cortex (vPMC), and the inferior frontal sulcus. To verify whether the ILOTC activated in the shape task was the same region as the LOtv reported in previous literature, we projected the peak coordinates of the LOtv from three representative studies (i.e., Amedi et al., 2001, 2002; Tal & Amedi, 2009) to the brain surface and found that these coordinates largely fell over the geometric gravity center of the ILOTC region. In

Figure 2A, we can identify two activity epicenters in the IPS—one was anterior, the other was posterior and joined to the intraoccipital sulcus.

The conceptual task mainly activated left-lateralized brain areas, including the anterior part of the lateral temporal lobe (aLTC), the superior temporal gyrus (STG; BA 22), the angular gyrus (AG; BA 39), and the supramarginal gyrus (SMG; BA 40). These regions were in accord with the high-level linguistic network (Fedorenko et al., 2011; Friederici, 2011) and are considered to underly language-supported conceptual processing (Xu et al., 2016, 2017).

We then looked at the brain activation in EB and SC separately (Figure 2B-C). Both EB and SC had ILOTC activation in the shape task compared to the conceptual task. To confirm that the regions in the ILOTC found in the two groups were the same, we calculated the overlap coefficient, i.e., the area of the intersection region divided by the smaller area of the two regions. The overlap coefficient of the left ILOTC was 100%, i.e., EB's ILOTC fell within SC's ILOTC. The overlap coefficient of the right ILOTC was 81.5%. Consistent with the results pooling all participants (N = 48), SC also had significant activation in bilateral aIPS, pIPS, and vPMC in the contrast between shape and conceptual tasks (Figure 2B). Although these regions did not survive the multiple comparison correction at the whole-brain level in EB (Figure 2C), analyses using the significant areas in SC as ROIs showed bilateral aIPS, bilateral pIPS, and the left vPMC in the EB also showed greater activation in the shape task than in the conceptual task (Supplementary Figure 1; left aIPS: $t(15) = 3.486$, $p = 0.003$; right aIPS: $t(15) = 2.487$, $p = 0.025$; left pIPS: $t(15) = 2.478$, $p = 0.026$; right pIPS: $t(15) = 3.357$, $p = 0.004$; left vPMC: $t(15) = 2.632$, $p = 0.019$; right vPMC: $t(15) = 1.861$, $p = 0.083$).

Both EB and SC activated the language network in the conceptual task. However, EB exhibited reduced left lateralization than SC. To measure the extent of lateralization, we extracted the T scores

of the top 5% percentage of vertices showing the strongest activation in the contrast between the conceptual task and the shape task within the language network, which was anatomically defined in each participant's native space by combing bilateral STG, bilateral inferior parietal cortices (i.e., the AG), and bilateral SMG in the DKT atlas (Klein & Tourville, 2012). The left lateralization was measured as (L − R) / (L + R), where L and R were the sums of T scores in the left and right hemispheres. While the SC had clear left lateralization ($M = 0.381$, $SD = 0.344$, $t(15) = 4.440$, $p < 0.001$), the EB's lateralization was not evident ($M = 0.143$, $SD = 3.397$, $t(15) = 1.442$, $p = 0.397$). The paired t-test showed a significant difference between the SC and the EB (paired $t(15) = 2.452$, $p = 0.027$), while no significant difference was found in handedness scores (SC: $M = 76.875$, $SD = 20.238$; EB = 73.750, SD = 16.279; paired $t(15) = 0.543$, $p = 0.595$). The reduced left lateralization for linguistic processing in EB has been reported in a recent study and is still open to interpretation (Lane et al., 2017).

Next, we directly contrasted the neural activity between EB and SC. As a sanity check, we first compared the brain activity level in the shape and conceptual tasks to the resting state between EB and SC. As both tasks included auditory input, the occipital cortex in EB should show enhanced activation due to cross-modal neuroplasticity, and the results showed up as expected (Supplementary Figure 2; vertex-wise $p < 0.001$, cluster-level FWE corrected $p < 0.05$). We then compared the activity level between the shape and conceptual tasks between EB and SC. We found only one significant region in the left cuneus near the parietooccipital sulcus (Figure 2D; vertex-wise $p < 0.001$, cluster-level FWE corrected $p < 0.05$). Region of interest (ROI) analysis showed that this region in EB had greater activation in the conceptual task than in the shape task ($t(15) = -3.447$, $p = 0.004$), whereas in SC, it showed an opposite pattern ($t(15) = 3.213$; $p = 0.006$). This finding demonstrates that the earlier "visual" cortex in EB, not the ILOTC, might repurpose itself to higher-level cognitive functions like conceptual processing.

Supplementary Figure 3A illustrates the RT effect across two tasks ($N = 48$; vertex-wise $p < 0.001$, cluster-level FWE corrected $p < 0.05$). As expected, it involved both frontoparietal and cingulo-opercular networks underlying top-down control (Dosenbach et al., 2008). It also involved regions in the default mode network, which could be because both the shape and the conceptual tasks require mental simulation (Buckner et al., 2008). Intriguingly, contrasting the RT effect between EB and SC revealed the lateral and ventral parts of the occipital cortex (Supplementary Figure 3B; vertex-wise $p < 0.001$, cluster-level FWE corrected $p < 0.05$). These regions substantially overlapped with the LOC involved in visual shape perception in the sighted population, suggesting a functional reorganization of these regions in EB. Note that these regions did not overlap with the ILOTC.

Other object properties did not modulate ILOTC activity.

To investigate whether the other object properties modulated brain activity in the ILOTC, we conducted a parametric modulation analysis. The set of the parametric modulators included the task type (i.e., the shape task coded as 1 and the conceptual task coded as -1), the z-scores of the RT across all the trials in each run, the rotated components corresponding to object size, toolness, touch experience, word duration, and word frequency. Figure 3 presents the significant brain areas encoding these parametric modulators ($N = 48$; vertex-wise $p < 0.001$, cluster-level FWE corrected $p < 0.05$).

When potential confounding factors were modeled, the difference between the two task types was still preserved (Figure 3A): The shape task activated bilateral brain areas, including the ILOTC, the aIPS, the pIPS, and the vPMC. The conceptual tasks mainly activated the language network in the left hemisphere, including the orbital part of the inferior frontal gyrus (IFG) (i.e., BA 47), the aLTC, the posterior part of the STG (pSTG), the SMG, and the AG. Since these brain clusters were more discrete

than those reported in the univariate contrast reported in Figure 2 (with no control for alternative object properties), we used the significant regions here to define the ROIs in the following analyses. No regions showed significant differences between EB and SC. We also found the same region in the cuneus when directly comparing EB and SC under a lower threshold (vertex-wise $p < 0.001$, uncorrected).

Figure 3B-C shows the brain areas sensitive to the other object properties. The object size was mainly localized to the three scene-selective regions—the transverse occipital sulcus, the parahippocampal place area, and the retrosplenial cortex (Figure 3B). It has already been reported that these areas also prefer large nonmanipuable objects (e.g., Konkle & Oliva, 2012; He et al., 2013) and objects with a strong contextual association (e.g., Bar & Aminoff, 2003; Kveraga et al., 2011). Since the object size component here had a moderate correlation with the rating scores on contextual association (Figure 1F), we cannot distinguish between these two factors in this study. Moreover, we found a region in the left ventral and medial temporal cortex (mainly in the BA 20), of which the level of activity negatively correlated to touch experience (Figure 3C), suggesting this region was sensitive to the novelty of objects. We did not find any brain areas significantly modulated by toolness, which might result from the lack of typical tools (e.g., hammer or scissor) in the stimuli. Directly comparing the effects of all these parametric modulators between EB and SC also failed to reveal any significant brain regions.

Supplementary Figure 4 illustrates the effect of the two linguistic variables ($N = 48$; vertex-wise $p < 0.001$, cluster-level FWE corrected $p < 0.05$). Word duration was localized to bilateral auditory cortices and bilateral STG. Word frequency was mainly localized to the right-lateralized ventral attention network and the salience network, characterized by their sensitivity to salient stimuli (e.g., Corbetta & Shulman, 2002; Seeley et al., 2007).

ILOTC represented shape similarity, not conceptual association in both EB and SC.

We then used representational similarity analysis (RSA) to investigate whether the ILOTC identified above implemented shape representation (Figure 3, left and right panels corresponding to left and right ILOTC). A three-way mixed ANOVA was first performed between Groups (EB vs. SC), Tasks (shape vs. conceptual tasks), and Representations (shape similarity vs. conceptual association). The Groups factor was between-subject, whereas Tasks and Representations were within-subject factors. In bilateral ILOTC, we only found a significant effect in the representational content and a significant interaction between Tasks and Representations (Table 2).

Figure 4A illustrates the RSA results in bilateral ILOTC across all participants (N = 48). Bilateral ILOTC represented shape similarity in both the shape task (left ILOTC: $t(47) = 10.367$, $p < 0.001$; right ILOTC: $t(47) = 7.705$, $p < 0.001$) and the conceptual task (left ILOTC: $t(47 = 4.066)$, $p < 0.001$; right ILOTC: $t(47) = 3.209$, $p = 0.002$). The shape representation was stronger in the shape task than in the conceptual task (left ILOTC: paired $t(47) = 5.183$, $p < 0.001$; right ILOTC: paired $t(47) = 3.776$, $p < 0.001$). We found no clear evidence that bilateral ILOTC represented the conceptual association in either the shape or the conceptual tasks—only the conceptual effect in the left ILOTC in the conceptual task was marginally significant ($t(47) = 2.123$, $p = 0.039$). No significant difference was found in conceptual representation between shape and conceptual tasks (left ILOTC: paired $t(47) = 0.558$, $p = 0.580$; right ILOTC: paired $t(47) = 0.395$, $p = 0.695$).

Figure 4B highlighted that the population without visual experience (i.e., the EB) showed a largely similar pattern. Bilateral ILOTC represented shape similarity in the shape task (left ILOTC: paired $t(15) = 4.568$, $p < 0.001$; right ILOTC: paired $t(15) = 3.610$, $p = 0.003$), whereas their shape representation in the conceptual task was less evident (left ILOTC: paired $t(15) = 1.220$, $p = 0.241$;

right ILOTC: paired $t(15) = 1.852$, $p = 0.084$). The paired t-test revealed a significant difference between the two tasks in the left ILOTC (paired $t(15) = 3.361$, $p = 0.004$) but not in the right ILOTC (paired $t(15) = 1.466$, $p = 0.163$). No evidence supported bilateral ILOTC represented conceptual association in either shape or conceptual tasks ($t(15) < 1.282$, $ps > 0.219$).

We also investigated whether bilateral ILOTC in EB and SC share a matched shape representation (Figure 4C). By doing so, we measured the within-group coherence—the correlation between each participant's Neural RDM and mean Neural RDM of the other participants within the same group (i.e., EB-EB and SC-SC), and the between-group coherence—the correlation between each participant's Neural RDM and mean Neural RDM of all the other participants in the other group (i.e., EB-SC). A two-way ANOVA was performed between Tasks (shape vs. conceptual tasks) and Group Pairs (EB-EB vs. SC-SC vs. EB-SC). No significant interaction was found between Tasks and Group Pairs (left ILOTC: $F(2,90) = 1.366$, $p = 0.260$; right ILOTC: $F(2, 90) = 1.446$, $p = 0.241$). There is a significant difference between tasks (left ILOTC: $F(1,90) = 90.743$, $p < 0.001$; right ILOTC: $F(1, 90) = 75.809$, $p < 0.001$), suggesting the shape task induced more coherent representations in bilateral ILOTC across participants. A weak effect in Group Pairs was also spotted in the left ILOTC ($F(2,90) = 4.746$, $p = 0.011$) but not in the right one ($F(2, 90) = 1.065$, $p = 0.349$). The post hoc comparison found that the mean value across levels of Tasks was significantly different between SC-SC and EB-EB (Tukey's test: $p = 0.011$), suggesting that the neural representation in the left ILOTC was more homogeneous in the SC group than in the EB group. However, there was no significant difference between EB-EB and EB-SC (Tukey's test: $p = 0.742$) or between SC-SC and EB-SC (Tukey's test: $p = 0.073$), suggesting there was no clear boundary effect between the neural representations across groups.

We averaged the Neural RDMs of bilateral ILOTC across all participants ($N = 48$) and provided a planar visualization of the representational pattern using multidimensional scaling (Figure 4D). The

color of words denoted the three clusters in the Model RDM of shape similarity, mainly corresponding to elongated, round, and square objects. Representations of the three shape categories were separated in bilateral ILOTC.

We also investigated the multivariate object representation in other regions showing an enhanced univariate response to the shape task than the conceptual task. Supplementary Tables 4-6 show the three-way mixed ANOVA results between Groups (EB vs. SC), Tasks (shape vs. conceptual task), and Representations (shape similarity vs. conceptual association) in bilateral aIPS, bilateral pIPS, and bilateral vPMC, respectively. They all had the same pattern, with a significant effect in Representations and a significant interaction between Tasks and Representations. Supplementary Figure 5 shows that all these regions represented shape similarity in the shape tasks ($t(47)$: 5.531-10.074, $ps < 0.001$). Bilateral aIPS and pIPS also represented shape similarity in the conceptual tasks ($t(47)$: 2.216-2.902, ps: 0.032-0.006), while shape representation in bilateral vPMC was not evident in the conceptual task (left: $t(47) = 1.875$, $p = 0.067$; right: $(47) = 1.677$, $p = 0.100$). Shape representation was more apparent in the shape task than in the conceptual task in all these regions (right vPMC: paired $t(47) = 2.602$, $p = 0.012$; other regions: paired $t(47)$: 0.408-5.055, $ps <= 0.001$).

Supplementary Figure 6A illustrated the whole-brain searchlight results of shape similarity in the shape tasks across all participants ($N = 48$) (vertex-wise FWE corrected $p < 0.005$, cluster size > 400 mm^2). The ILOTC was one of the epicenters showing the strongest shape effect. Direct contrast between EB and SC revealed a region in the right lateral occipital cortex showing a stronger shape representation in the EB than SC (Supplementary Figure 6B; vertex-wise $p < 0.001$, cluster-level FWE corrected $p < 0.05$).

Conceptual representation in the brain

We also used the RSA to investigate whether the brain areas sensitive to the conceptual task in the univariate analyses represented multivariate conceptual association (Figure 5). Interestingly, although all these regions showed significantly stronger univariate activation in the conceptual task than in the shape task, only the left AG represented the conceptual association in the conceptual task across all the participants (orbital IFG: $t(47) = 2.395$, $p = 0.021$; aLTC: $t(47) = -1.268$, $p = 0.211$; pSTG: $t(47) = -0.621$, $p = 0.537$; AG: $t(47) = 3.337$, $p = 0.002$, SMG: $t(47) = 1.174$, $p = 0.246$; only the AG survived from multiple comparison correction: Bonferroni corrected $p = 0.01$). The conceptual representation in the left AG was more evident in the conceptual task than in the shape task (paired $t(47) = 2.163$, $p = 0.036$), and no group difference were found between EB and SC ($F(1, 30) = 0.192$, $p = 0.664$).

Supplementary Figure 7 illustrated the whole-brain searchlight results of conceptual association in the conceptual tasks across all participants ($N = 48$) (vertex-wise $p < 0.001$, cluster-level FWE corrected $p < 0.05$). The effects were mainly on bilateral dorsal AG, the left pIPS, the left precuneus, and the frontal regions. Given that some of the regions could also be spotted in the shape effect in the shape task (Supplementary Figure 6A), they were likely to be driven by the task context (Bracci et al., 2017).

Shape and conceptual brain network in both EB and SC

We last used the seed-based RSFC to trace the regions having the neural activity synchronized with bilateral ILOTC (left ILOTC: Figure 6A; right ILOTC: Figure 6B; vertex-wise FWE corrected $p < 0.005$, cluster size > 400 mm^2). The ILOTC had strong RSFC to the other bilateral regions sensitive to the shape task—the aIPS, the pIPS, and the vPMC in both EB and SC. The left ILOTC in EB had stronger connectivity to the "visual" cortex than in SC (Supplementary Figure 8; vertex-wise $p < 0.001$, cluster-level FWE corrected $p < 0.05$).

Figure 6C illustrates the mean RSFC matrix across participants in EB and SC among the regions showing stronger activation in the shape tasks or in the conceptual task. It shows that the brain areas sensitive to the shape task and those sensitive to the conceptual task belonged to separate network modules in both EB and SC. Figure 6D further compares the mean RSFC across all the pairs among the shape-sensitive regions, among the conceptual-sensitive regions, and between the shape- and the conceptual-sensitive regions. In both EB and SC, the mean RSFC within the shape module (EB: paired $t(15) = 10.650$, $p < 0.001$; SC: paired $t(15) = 9.563$, $p < 0.001$) and within the conceptual module (EB: paired $t(15) = 10.024$, $p < 0.001$; SC: paired $t(15) = 8.014$, $p < 0.001$) was significantly stronger than the mean RSFC between the two network modules.

Discussion

Our study investigated where and how shape representation are stored in the brain and distinguished from the conceptual representation of the same manmade objects. By testing early blind participants, we assessed whether occipital regions implement shape representation independently of visual experience/imagery (e.g., Amedi et al., 2005; Lacey et al., 2009; Ricciardi et al., 2014) or, alternatively, whether the "visual" cortex would repurpose its function for conceptual representation due to early visual deprivation (Bedny, 2017). We found that bilateral lLOTC, a region that overlaps with the LOtv (Amedi, 2001; 2002; Tal & Amedi, 2009), together with bilateral aIPS, pIPS, and vPMC, showed greater activation when people process shape rather than conceptual attributes of the same name of objects, and their activity pattern encoded shape similarly but not conceptual association among objects. In contrast, regions in the left perisylvian area, including the orbital IFG, the aLTC, the pSTG, the AG, and the SMG, showed greater activation in the conceptual task than in the shape task. RSFC analysis further demonstrated that shape- and conceptual-relevant regions formed distinct brain networks. Interestingly, in all the above results, visual experience had little influence—EB and SC had similar activity profiles and connectivity patterns.

Our results thus favor the hypothesis suggesting the lLOTC implements supramodal shape representation and reject the alternative hypotheses that such activation depends on visual imagery or conceptual processing. These results echoed various perspectives suggesting object representation in the brain is organized according to properties, not modalities (e.g., Pascual-Leone & Hamilton, 2001; Ricciardi et al., 2014; Martin et al., 2016).

In contrast to the view that lLOTC implements supramodal shape representation, one could argue that this region might represent visual shapes in the sighted and haptic shapes in the early blind. Testing

this possibility using fMRI is challenging as it is difficult to distinguish supramodal representation and visual representation derived from visual imagery triggered by touch in the sighted participants. One option would be to examine whether the sighted patients with bilateral lesions in the ILOTC have both visual and tactile shape agnosia or only visual shape agnosia. Unfortunately, the two existing cases of bilateral ILOTC lesions cannot convincingly answer this question. One case is patient D.F., who had bilateral lesions in the LOC (James et al., 2003) and had both visual and tactile agnosia (James et al., 2006). However, D.F. also had bilateral lesions to the parieto-occipital cortex (Bridge et al., 2013), and her tactile agnosia might result from parietal damage. The other case is patient M.C., who had bilateral lesions in the LOC, including the LOtv (Snow et al., 2015). Unlike D.F., M.C. only had visual agnosia, and her tactile recognition ability was fast and accurate. However, although the haptic shape task did not activate the ILOTC of M.C. due to lesions in this region, it activated a nearby region in the posterior middle temporal gyrus. Such activation might reflect post-lesion reorganization, compensating for the shape representation that should be implemented in the ILOTC (Snow et al., 2015). Besides resorting to rare patient cases, another seemingly plausible option would be selective transcranial magnetic stimulation (TMS) over bilateral ILOTC to evaluate whether it interferes with both haptic and visual shape tasks or only visual shape tasks. However, the pitfall is that even if TMS over bilateral ILOTC does disrupt haptic shape tasks (e.g., longer reaction time), such disruption might be mediated by the disruption in visual imagery, a strategy sighted participants would adopt to facilitate haptic shape tasks (e.g., Lederman et al., 1990; Zhang et al., 2004).

While conclusive proof is still warranted, converging evidence supports the role of ILOTC in supramodal shape representation in the sighted population. On the one hand, the ILOTC (mainly in BA 37) is anterior to the lateral occipital cortex (LO, mainly in BA 18), which is engaged in visual shape perception. According to embodied semantic theories (Barsalou et al., 2003) and the "anterior shift" phenomenon noted first by Thompson-Schill (2003), the associate cortex anterior to each

532 sensorimotor area can gradually capture the regularities of the activity patterns in its nearby
533 sensorimotor cortices induced by different exemplars of the same concept (e.g., different exemplars of
534 an apple) and generate a schema-like representation as the sensorimotor knowledge of that concept
535 (e.g., the typical color, shape, and action related to an apple). In line with this hypothesis, the region
536 representing objects' color knowledge is localized to the fusiform gyrus anterior to the color perception
537 area in V4 (Miceli et al., 2001; Simmons et al., 2007), and language-induced category-specific
538 activations are aligned with but anterior to the visual-induced activations of the same semantic
539 category (Popham et al., 2021). The ILOTC thus might represent objects' shape knowledge derived
540 from the visual shape perception process in the LO of sighted people.
541
542 On the other hand, previous studies have shown that the ILOTC is sensitive to pictures of hands over
543 other body parts and pictures of graspable tools over non-graspable manmade objects (e.g., Bracci et
544 al., 2013), suggesting this region might be involved in extracting supramodal object's shape
545 information for grasping. In our study, we found that the ILOTC was strongly connected to the IPS
546 and the vPMC (Figure 5), a frontoparietal circuit that has long been proposed to be involved in grasping
547 objects (see reviews by Jeannerod et al., 1995; Castiello et al., 2005). Neuropsychological evidence
548 shows that lesions in the aIPS can induce both tactile shape agnosia (Hömke et al., 2009) and tactile
549 apraxia (Binkofski et al., 2001), and lesions in the vPMC can lead to syndromes resembling tactile
550 apraxia (Dettmers et al., 2003). Our study found that the IPS-vPMC circuit implemented shape
551 representation even in the early blind population with no visual experience (Supplementary Figure 1,
552 Supplementary Tables 4-6), further demonstrating that haptic sources alone can form the shape
553 representation in these regions.
554
555 Converging the two groups of evidence described above—the position in the ventral visual pathway
556 and the connection to the frontoparietal haptic circuit, it appears parsimonious to postulate that the

ILOTC act as an operator bridging visual and haptic shape representations. As the shape representation in the ILOTC is sensorimotor-derived, the format of such representation would still be analogical instead of amodal symbolic, which is usually supported by the language system (e.g., the symbol of a "ring" associated with the symbol of "round") (e.g., Paivio, 1986; Bi, 2021). Nevertheless, the supramodal shape representation in the ILOTC should be more abstract than the topographic representation in the earlier sensorimotor cortex (e.g., retinotopy) and can be shared across modalities. Recent studies have shown that the activity pattern in the LO—the visual shape perception region posterior to the ILOTC—were significantly correlated to shape curvatures (Vernon et al., 2016). It is thus possible that the ILOTC might also represent curvature information but independently of specific senses.

As for the neural representation of functional knowledge, contrasting the conceptual task with the shape task revealed the left perisylvian regions related to linguistic processing (Figure 2 and Figure 3), implying that function knowledge is supported by the language system. This result is supported by a recent massive study with 136 acute left-hemisphere stroke patients (Martin et al., 2016). They found that the deficit in tool selection (e.g., choosing the nail for the hammer) was specifically related to lesions in the left perisylvian regions, mainly including the whole length of the lateral temporal lobe and the anterior IFG. The language system might provide a symbolic format of representations, which can better capture the abstract "associations" among holistic concepts. It contrasts with the analogical format of representation grounded in the sensorimotor system (as discussed for the shape representation in lLOTC), which can better reflect the "similarity" in one particular semantic feature. Such findings suggest that function is not an explicit object property, which can be directly derived from sensorimotor experience—we cannot reduce an objects' function to what it looks like and how it is manipulated; it must therefore rely on some sort of abstract/linguistic coding.

582 The differences between these two neural coding mechanisms may explain the discrepancy in the RSA
583 results between shape similarity and conceptual association. RSA assumes that the representational
584 content can be inferred from the distributed activity pattern across cortical surfaces. The most
585 definitive evidence supporting this assumption comes from the primary sensorimotor system following
586 a topographic organization (e.g., retinotopy), where the input and output information is transparently
587 projected to the cortical surface. Since the shape representation (e.g., curvatures) is transited and
588 abstracted from the topographic representation (Vernon et al., 2016), the activity pattern across the
589 cortical surface in the shape-relevant regions would still be informative. However, in the linguistic
590 system, the representation is presumed to be coded in the format of "arbitrary" symbols, where the
591 linguistic sign (e.g., word forms) bears no obvious resemblance to the content signified. The content
592 represented in the language system thus is not directly transited or abstracted from the word form
593 representations in the sensorimotor cortex and might not be transparently reflected on the activity
594 pattern across the cortical surface. Our results confirmed this hypothesis. Whereas all the shape-
595 relevant regions defined by the univariate contrast encoded the shape similarity among objects (Figure
596 4; Supplementary Figure 5), among the conceptual-relevant regions defined by the univariate contrast,
597 only the activity pattern in the AG was correlated to the conceptual association RDM (Figure 5).
598 Previous studies have shown that the AG is not a purely linguistic region but also part of the default
599 mode network engaged in memory-based simulation (e.g., Buckner et al., 2008; Xu et al., 2016, 2017).
600 Compared to the other linguistic regions, the AG is less responsive to word forms (e.g., Graves et al.,
601 2022) but more sensitive to the retrieval of multimodal episodic memories (e.g., see reviews by
602 Humphrey et al., 2021). It is thus possible that the AG codes thematic relations based on the
603 spatiotemporal continuity in our sensorimotor experience (e.g., hammers and nails often co-occur;
604 Mirman et al., 2017), which is apt to reflect on activity patterns (Xu et al., 2018), in contrast to the
605 coding based on linguistic associations in the other language areas.
606

Our study also reveals crucial neuroplastic principles about how the "visual" cortex reorganizes its function after vision loss. In the high-order visual cortex, where brain areas receive not only visual input but also information from other sensorimotor systems, brain functions are likely to be resilient to vision loss through compensation. The most well-documented example is the region hMT+/V5, a highly specialized area for visual motion processing. This region also has a direct white-matter connection to the planum temporale specialized in auditory motion processing (Gurtubay-Antolin et al., 2021) and preferentially responds to moving auditory and tactile stimuli in the early blind (e.g., Poirier et al., 2006; Ricciardi et al., 2007; Ptito et al., 2009; Dormal et al., 2016, Battal et al., 2022). Our results reveal the ILOTC has a similar nature—it had strong connections to the frontoparietal regions involved in haptic processing and preserved its functionality despite the lack of visual input (Figure 2 and Figure 4). In contrast, in more primary visual cortex, where visual input is dominant, vision loss will leave a functional vacancy that would be difficult for another sense to remap. Higher-order brain systems might have the opportunity to take over, pushing for a more radical functional repurposing in those early visual regions. This hypothesis is supported by neuroimaging studies showing that part of the "visual" cortex of the early blind is sensitive to linguistic components (semantics and syntax; e.g., Bedny et al., 2011; Lane et al., 2015; Van Ackeren et al., 2018) and mathematical difficulty (Kanjlia et al., 2016). In line with these findings, we found that the left cuneus in EB showed greater activation to the conceptual task than the shape task, whereas the same conceptual preference can only be observed in the left perisylvian linguistic areas in SC (Figure 2). Similarly, the lateral occipital cortex and the posterior fusiform gyrus in EB—two “earlier” regions along the visual processing stream than the ILOTC—showed a domain-general RT effect, which is typically observed in the frontoparietal and cingulo-opercular areas in SC (Supplementary Figure 2).

To conclude, our study identified dissociable brain networks representing objects' shape and conceptual knowledge. The bilateral ILOTC-IPS-vPMC circuit represented shape knowledge, and the

632 left perisylvian circuit related to language processing represented conceptual knowledge. Relying on
633 data collected in EB, we highlighted that the ILOTC represents shape knowledge independently of
634 visual experience. We argue that the ILOTC implement a supramodal shape representation by virtue
635 of its position in the ventral visual pathway and its strong connections to the IPS-vPMC circuit
636 involved in haptic processing, and such sensorimotor-derived representation differs from the
637 disembodied representation supported by the language system in their representational formats.
638

Materials and Methods

Participants

Forty-eight native Italian speakers with no history of neurobiological or psychiatric disorders participated in the fMRI experiment. Thirty-two participants were sighted, and sixteen participants were early blind. Further recruitment of the blind participants was stalled due to Covid-19 restrictions. The early blind (EB) group reported, at most, faint light perception and had no visual memories (10 females; age: M = 32.8, SD = 4.5; all right-handed). To match the demographic information of the early blind group, we divided the sighted participants into two groups. Sixteen formed the sighted control (SC) group, matching the early blind in pairs on gender and age (10 females; age: M = 32.5, SD = 5.9; all right-handed). There was no significant difference between the early blind and the sighted control in head motion measured by the mean framewise displacement index (Power et al., 2012) (early blind: M = 0.20 mm, SD = 0.05 mm; sighted control: M = 0.17 mm, SD = 0.06 mm; $t(30) = 1.79$, $p = 0.083$). The other sixteen formed the independent sighted (IS) group (seven females; age: M = 28.3, SD = 8.1; two left-handed). We investigated the group-general effect by pooling EB, SC, and IS together to increase the statistical power. We investigated the between-group difference by contrasting EB and its matched SC.

Supplementary Table 1 shows the demographic information of the early blind and their matched sighted control. In each matched pair, the gender was the same, and the age difference was no more than three years. All blind participants were blind since birth except for three participants, who also had visual trouble since birth but fully lost their vision at eight months, two years, and four years. These participants' data did not differ from those of the other blind participants.

664 The ethical committee at the University of Trento approved the experimental protocol in this study.
665 All participants provided written informed consent and were paid for their time.
666
667 *Stimuli*
668
669 To disentangle shape and conceptual representation, we aimed to select a set of words referring to
670 objects among which the pairwise shape similarity was orthogonal to the pairwise conceptual
671 association.
672
673 Here, we differentiated two types of conceptual relations. One assumes concepts are componential,
674 consisting of a set of shared semantic features (e.g., shape, action, motion, and emotion); similarity
675 across semantic features leads to taxonomic relations and categories (e.g., forks and knives are
676 manmade objects, not animals). The other assumes concepts are holistic; complementary roles within
677 the same scenario lead to thematic relations and categories (e.g., folks and knives relate to eating, not
678 sleeping). This study focused on thematic relations by confining its stimuli to one taxonomic
679 category—manmade objects, based on the following considerations: (1) Growing evidence suggests
680 taxonomic and thematic relations rely on dissociable mental and neural systems (e.g., Mirman et al.,
681 2017; Xu et al., 2018). Confusing them might be problematic. (2) It is hard to tell whether a brain area
682 represents taxonomic relations or the distinguishing features of one particular taxonomic category. For
683 example, mainly manmade objects have manipulation-related features, large still objects have
684 locational features, and humans have social features. Brain areas representing these particular semantic
685 features will also exhibit taxonomic differences. (3) Shape features, which we aimed to disentangle
686 from conceptual knowledge, per se, contribute to forming taxonomic relations. (4) Compared to the
687 sighted, the early blind lack perceptual experience with many concepts in the natural world and have

different neural representations of these "imperceptible" concepts (Striem-Amit et al., 2018). Using only manmade objects ensures a relatively fair comparison between the sighted and the early blind.

As a starting point, we preselected a set of Italian words referring to 60 everyday manmade objects based on our subjective impressions so that, among these objects, the shape similarity did not always correlate to the conceptual association. For example, a plate ("piatto") is perceptually similar to a coin ("moneta") but conceptually relates to a fork ("forchetta").

Next, we recruited 19 sighted native Italian speakers (age: M = 25.4, SD = 3.6) who did not participate in the fMRI experiments to rate the shape similarity and the conceptual association among the 60 objects. As pairwise rating among numerous items is time-consuming (60 objects requires 1770 pairs of comparison), we adopted the multi-arrangement method (Kriegeskorte & Mur, 2012). By doing so, participants arranged Italian words on a computer screen by mouse drag-and-drop operations in two 45 min task sessions. The closeness among the words was required to reflect shape similarity in the shape task session and conceptual association in the conceptual task session. Participants were instructed to disregard other object properties like color and size. The pairwise dissimilarity matrix of shape and conceptual information was estimated as the weighted mean of the scale-adjusted on-screen distances from individual arrangements. We averaged the ratings across participants and obtained a mean pairwise dissimilarity matrix for shape and conceptual information, respectively.

Then, these participants rated the potential confounding factors, i.e., object size (big vs. small), toolness (tools vs. non-tool manmade objects), and contextual association (strong vs. weak contextual association objects). Participants were instructed to rate these three unidimensional variables by sliding a horizontal slider from left to right on a computer screen. To assess the variance in familiarity across objects, participants also rated each object on a 7-point Likert scale about the degree to which they

713 knew its typical shape and primary function (1: do not know it at all; 7: know it very well). We also
714 conducted a telephone interview with 16 early blind participants (eight females; age: M = 33.0, SD =
715 6.6; six of the participants took part in the fMRI experiment). We let them perform the same shape and
716 conceptual familiarity rating tasks and asked them whether they had ever touched the objects. We
717 averaged the rating score across participants to obtain a mean rating score for each object and each
718 rating task.
719
720 After that, we selected 21 from the 60 Italian words based on the above ratings. This set of words met
721 the following criteria: (1) Both sighted and early blind participants knew each object's typical shape
722 and primary function. The shape and the conceptual familiarity rating scores were higher than 5.8 (7-
723 point Likert scale) in both groups. (2) Most early blind participants we interviewed (i.e., at least 14
724 among 16 participants) had touched the objects. (3) Shape similarity and conceptual association were
725 orthogonal across pairs of objects. The absolute value of Spearman's correlation coefficient was 0.039.
726 (4) Both shape similarity and conceptual association were orthogonal to the potential confounding
727 factors, including both shape and conceptual familiarity from both early blind and sighted participants,
728 word length (i.e., number of letters), word frequency (i.e., the Zipf value of the word occurrence in
729 film and television subtitles; http://crr.ugent.be/subtlex-it/), object size, toolness, and contextual
730 association. Since all these confounding factors were unidimensional, we measured the pairwise
731 dissimilarity of these variables as the absolute difference between each pair of objects and correlated
732 it to the shape and the conceptual information, respectively. The absolute values of Spearman's
733 correlation coefficients were all below 0.15. (5) The variances across pairwise shape similarity
734 (variance = 0.54) and pairwise conceptual association (variance = 0.53) were maximized while kept
735 comparable. (6) Each object had at least one shape-matched item and one conceptual-associated item.
736 Supplementary Table 2 shows the 21 Italian words and their English translation.
737

738 Finally, a professional narrator recorded his pronunciation of these 21 words. We cut out the silence
739 period at the beginning and the end of each auditory word with the same threshold and equalized the
740 average intensity of all the auditory words as 70 dB using Praat 6.1.01
741 (https://www.fon.hum.uva.nl/praat/).
742
743 *Procedures*
744
745 Before the fMRI scanning, all participants rated each object on a 7-point Likert scale about the degree
746 to which they knew its typical shape and primary function (1: do not know it at all; 7: know it very
747 well). They also rated how frequently they touched each object (1: have never touched it before; 7:
748 touch it every day). We then explained the items of which either shape or conceptual familiarity rating
749 score was below 6 points to ensure that all participants knew each object's typical shape and primary
750 function. Supplementary Text 1 shows the survey questions of these ratings.
751
752 During the fMRI scanning, we presented audio stimuli using Psychotoolbox-3
753 (http://psychtoolbox.org/). The sound was delivered through in-ear headphones. Before the formal
754 scanning, we adjusted the volume for each participant so that they could hear the pronunciation clearly
755 under the scanning noise but did not feel too loud. To ensure both sighted and blind participants
756 received the same input during the scanning, we blindfolded all participants and turned off the lights
757 in the scanning room.
758
759 The scanning session included one resting-state run at the beginning (8 min), ten task-state runs (5 min
760 30 s each), and one run collecting T1 weighted images after the first five task-state runs. During the
761 resting-state run, participants were instructed to keep their heads still, not fall asleep, and not think

about particular things. During the task-state runs, participants performed verification tasks on the words they heard.

Each task-state run was divided into two even blocks. One corresponded to the shape verification task, and the other corresponded to the conceptual verification task. The order of the two task blocks was interleaved across runs within each subject, and the order in the first run was counterbalanced across subjects within the early blind and the sighted control group. Each block started with a 10 s rest, followed by a 20s task probe. In the shape verification block, we instructed participants to think carefully about objects' shape ("Pensa attentamente alla forma") and judge whether they were elongated ("allungato"), angular ("angolare"), hollow ("cavo"), circular ("circolare"), and discal ("discoidale"). In the conceptual verification block, we instructed participants to think carefully about objects' function ("Pensa attentamente alla funzione") and judge whether they were used for eating ("per mangiare"), writing ("per scrivere"), sleeping ("per dormire"), lighting ("per illuminazione"), and purchasing ("per fare acquisti"). These five shape and conceptual verification tasks were randomly assigned to each participant's first five task-state runs, and the second five task-state runs repeated these tasks in the same order. In this way, gaps between the same tasks were evenly distributed, and the same tasks could not be repeated in close time proximity. Participants made a yes/no judgment by pressing buttons using their right index/middle fingers. To counterbalance the motor effects of different fingers, we instructed each participant to switch the correspondence between yes/no judgments and index/middle fingers in the second five runs.

Each block included 21 trials after the task probe, with 21 words presented once. Each trial started with a 100 ms beep to capture participants' attention, followed by a 300 ms silence and an auditory word (word duration: M = 662 ms, SD = 165 ms). The stimulus onset asynchrony was jittered as either 5 s or 8 s—eleven trials lasted 5 s, and ten trials lasted 8 s. The order of the words and the jitter intervals

were randomized for each block. Participants were instructed to press buttons within 5 s after the stimulus onset. The reaction time was measured as the interval between the stimulus onset and the button press.

After the fMRI scanning, participants also rated object properties. For pairwise shape similarity and pairwise conceptual association, we adapted the paradigm for both sighted and blind populations by presenting the stimuli in the auditory modality. In each trial, participants heard two words in sequence and rated on a 7-point Likert scale (for shape rating, 1: not similar at all, 7: identical in shape; for conceptual rating, 1: not associated at all, 7: strongly associated). Both rating tasks consisted of 210 trials covering all the possible object pairs. For the other three object properties as potential confounding factors, participants rated item-wise on a 7-point Likert scale. They were object size (1: as small as a needle, 7: as big as a television), tool-ness (1: nontools like a lamp, 7: tools like a hammer), and conceptual association (1: weak contextually associated like a cellphone, 7: strong contextually associated like a bowling ball). Supplementary Text 1 shows the survey questions of these ratings.

Behavior analysis

For pairwise shape similarity and conceptual association ratings, we averaged the rating scores across all participants who took part in the fMRI experiment and calculated the Model RDMs for the following representational similarity analysis (i.e., 7 minus the mean rating score). To investigate the organizational structure of the two Model RDMs, we performed the clustering analysis using the k-means clustering algorithm (Lloyd, 1982; Vassilvitskii & Arthur, 2006). The maximum number of iterations was 10000, the number of times to repeat clustering using new initial cluster centroid positions was 100, and the silhouette criterion was adopted to decide the optimal number of clusters in

the range from 2 to 10 (Rousseeuw, 1987). We conducted this analysis using the *kmeans* and *evalclusters* function in Matlab 2021.

For the ratings on other object properties (i.e., object size, contextual association, and toolness) and touch experience, we averaged the rating scores across all participants to obtain a mean vector for each rating item. These mean rating vectors, together with word duration and word frequency, constituted the potential confounding factors. To investigate the effect of these factors in the subsequent parametric modulation analysis, we orthogonalized these unidimensional variables using principal component analysis. Varimax rotation was applied to increase the interpretability of components, and five rotated components of which the eigenvalues were greater than 1 were selected. The principal component analysis was performed using the *principal* function in the R package *psych 2.1.9.*

Analyses on the performance during fMRI scanning were made using JASP (Version 0.16).

MRI acquisition

MRI data were acquired using a MAGNETOM Prisma 3T MR scanner (Siemens) with a 64-channel head-neck coil at the Centre for Mind/Brain Sciences, University of Trento. Functional images were acquired using the simultaneous multislices echoplanar imaging sequence: the scanning plane was parallel to the bicommissural plane, the phase encoding direction was from anterior to posterior, repetition time (TR) = 1000 ms, echo time (TE) = 28 ms, flip angle (FA) = 59°, multiband factor = 5. All participants in the early blind and sighted control groups and seven participants in the independent sighted group used a 3 mm spatial resolution: field of view (FOV) = 198 mm × 198 mm, matrix size = 66 × 66, 65 axial slices, slices thickness (ST) = 3 mm, gap = 0.3 mm, voxel size = 3 × 3 × (3 + 0.3) mm. The rest nine participants in the independent sighted group used a 2 mm spatial resolution: FOV

836 = 200 mm × 200 mm, matrix size = 100 × 100, 65 axial slices, ST = 2 mm, gap = 0.2 mm, voxel size
837 = 2 × 2 × (2 + 0.2) mm. Three-dimensional T1-weighted images were acquired using the
838 magnetization-prepared rapid gradient-echo sequence, sagittal plane, TR = 2140 ms, TE = 2.9 ms,
839 inversion time = 950 ms, FA = 12°, FOV = 288 mm × 288 mm, matrix size = 288 × 288, 208 continuous
840 sagittal slices, ST = 1 mm, voxel size = 1 × 1 × 1 mm.
841
842 *MRI preprocessing*
843
844 We performed MRI preprocessing using fMRIPrep 20.0.5 (Esteban, Markiewicz, et al. 2018; RRID:
845 SCR_016216), based on Nipype 1.4.2 (Gorgolewski et al. 2011; RRID: SCR_002502). Please see
846 Supplementary Text 2, a boilerplate text directly generated by the fMRIPrep. It describes the detailed
847 preprocessing steps used in the current study, aiming for a clear and consistent description to improve
848 experimental reproducibility.
849
850 As surface-based analysis can significantly improve the spatial localization compared to the traditional
851 volume-based analysis (Coalson et al., 2018), we analyzed the images in the surface space generated
852 by fMRIPrep (i.e., the fsaverage5 or the fsnative space). We conducted the surface smoothing of the
853 functional images with a full width at half maximum (FWHM) of 6 mm using the mri_surf2surf
854 command in FreeSurfer (http://surfer.nmr.mgh.harvard.edu/).
855
856 *First-level neuroimaging analysis*
857
858 We performed the first-level analysis using SPM12
859 (https://www.fil.ion.ucl.ac.uk/spm/software/spm12/). Individual-level general linear models (GLMs)
860 were built separately for univariate contrast, parametric modulation, and representational similarity

861 analyses. In all three GLMs, six rigid-body transformation parameters and constant variables
862 indicating each of the ten runs were involved as nuisance regressors. A high-pass filter with a cutoff
863 of 512 s was used to remove low-frequency noise and slow drifts. The RSA used unsmoothed images,
864 while the other two analyses used smoothed images.
865
866 The GLM for the univariate contrast analysis involved three events—the shape task, the conceptual
867 task, and the task probe. The duration of shape and conceptual tasks was set as each trial's RT, and the
868 duration of task probes was set as the auditory period before each block introducing the task ahead.
869 The resulting boxcar function was convolved with a canonical hemodynamic response function (HRF).
870 In this way (i.e., the variable epoch approach), the trial-by-trial RT variability was modeled (Grinband
871 et al., 2008). To further control the domain-general effect of RT across the two tasks, we also used
872 stick functions to model the trial-by-trial RT variability. We pooled the trials in the two tasks together,
873 modulated the amplitude of sticks by the mean-centered RT, and convoluted the RT-modulated stick
874 function with the canonical HRF (i.e., the variable impulse approach). The resulting RT variable was
875 involved in the GLM as one regressor. We contrasted the shape task, the conceptual task, and the RT
876 regressor to the resting state and contrasted between shape and conceptual tasks. The obtained
877 combined beta images were used in the second-level analysis.
878
879 The GLM for the parametric modulation analysis only involved two conditions—the trials (i.e., shape
880 and conceptual tasks pooled together as one condition) and the task probes. The duration of trials was
881 set as its RT, and the duration of task probes was set as the auditory period before each block
882 introducing the task ahead. We modulated the condition of the trials with a set of parametric variates,
883 including the task type (i.e., the shape task coded as 1 and the conceptual task coded as -1), the z-
884 scores of the RT across all the trials in each run, the rotated components corresponding to word
885 duration, word frequency, object size, toolness, and touch experience. The option for orthogonalizing

886 modulations in the SPM was turned off (Mumford et al., 2015). We contrasted each parametric
887 modulator to zero. The obtained combined beta images were used in the second-level analysis.
888
889 The GLM for the RSA involved each word in each task as a separate condition and the task probes as
890 one condition. Following Kriegeskorte et al. (2008), we concatenated ten runs to improve the reliability
891 of the model estimation. The duration of trials was set as its RT, and the duration of task probes was
892 set as the auditory period before each block introducing the task ahead. The trial-by-trial RT variability
893 across two tasks was also modeled using the variable impulse approach. We contrasted each word in
894 each task to the resting state. The obtained T images instead of the beta images were used in the
895 following RSA (Misaki et al., 2010).
896
897 *Representational similarity analysis*
898
899 The RSA was conducted among the 21 object conditions within shape and conceptual tasks separately.
900 It included two steps of correlations (Kriegeskorte et al., 2008). In the first-order correlation, we
901 calculated the Spearman distance of the activity patterns across vertices between each pair of
902 conditions and obtained a 21 × 21 Neural RDM for a particular region. In the second-order correlation,
903 we correlated the Neural RDM and each Model RDM (i.e., shape similarity and conceptual association)
904 across the 210 pairs using Spearman correlation. The resulting correlation coefficients were Fisher z-
905 transformed using the inverse hyperbolic function.
906
907 The ROI-based RSA focused on two sets of ROIs derived from significant brain areas in the second-
908 level of the parametric modulation analysis (see below). The shape ROIs were bilateral and had
909 significantly greater activation in the shape task than in the conceptual task—the ILOTC, the aIPS, the
910 pIPS, and the vPMC. The conceptual ROIs were left-lateralized and were significant in the opposite

911 contrast—the orbital IFG, the aLTC, the pSTG, the AG, and the SMG. In cases when clusters were
912 stuck together under the conventional threshold (vertex-wise $p < 0.001$, cluster-level FWE corrected p
913 < 0.05), we raised the vertex-wise threshold until they were isolated.
914
915 The searchlight-based RSA was performed to provide a global view of the results (Kriegeskorte et al.,
916 2006). The searchlight spot went through all the vertices on the fsaverage5 surface. For each vertex,
917 the spot included the six vertices directly connecting to the central vertex and the more peripheral
918 vertices connecting to the six vertices (i.e., 19 vertices in total) (Zuo et al., 2013). The Fisher z-
919 transformed second-order correlation coefficient was assigned back to the central vertex, and a surface
920 smoothing with a 6 mm FWHM was applied on the resulting maps.
921
922 To investigate whether the ILOTC in EB and SC represented the same content, we compared the inter-
923 subject neural RDM correlation within the same group (i.e., EB-EB and SC-SC) and between different
924 groups (i.e., EB-SC). The within-group inter-subject correlation was calculated in a leave-one-subject-
925 out manner. The neural RDM of the ILOTC of one participant was correlated to the mean neural RDMs
926 of all the other participants within the same group across the 210 object pairs. This procedure ended
927 up with 16 correlation coefficients for each group. The between-group inter-subject correlation was
928 calculated in two steps. First, the neural RDM of the ILOTC of one participant in one group was
929 correlated to the mean neural RDMs of all the participants in the other group across the 210 object
930 pairs, which generated 16 correlation coefficients for each group. Second, we averaged the correlation
931 coefficients from the EB and SC participants in the same pair to obtain 16 between-group correlation
932 coefficients. These correlation coefficients were calculated using Spearman's correlation and were
933 Fisher z-transformed.
934

To provide a planar visualization about the representational pattern in bilateral ILOTC in the shape task, we performed the multidimensional scaling analysis using the *mdscale* function in Matlab 2021. The input dissimilarity matrix was the mean Euclidean distance between each pair of conditions averaged across all participants (N = 48). We used the squared stress, normalized with the sum of 4^{th} powers of the dissimilarities, as the goodness-of-fit criterion to minimize.

Resting-state functional connectivity

We started from the unsmoothed resting-state images. To remove nonneuronal nuisance variables, we built a GLM to predict the timecourse of each vertex using the 24 head motion regressors (Friston et al., 1996), the mean timecourses in a conservative mask of the white matter and the cerebrospinal fluid extracted by the fMRIPrep, and the linear trend with the time points. We estimated the beta coefficients using the *fitglm* function in Matlab 2021 and subtracted all the terms (i.e., the dot product of all the nuisance variables and their estimated beta coefficients) from the original timecourses. A band-pass filter (0.01-0.1 Hz) was then performed on the resulting timecourses using the infinite impulse response filter method, and surface smoothing was carried out with a 6 mm FWHM. The functional connectivity between two regions was defined as the Pearson's correlation between their timecourses. The correlation coefficients were Fisher z-transformed before the second-level analysis. The ROIs used in the seed-based RSFC and the interregional RSFC also came from the parametric modulation analysis.

Second-level neuroimaging analysis

We performed the group-level one-sample t-test or two-sample t-test (i.e., EB vs. SC) on the first-level beta images from the univariate contrast and parametric modulation analyses, the searchlight-based

RSA images, and the RSFC images. The statistic inference was made using the permutation method with PALM (https://fsl.fmrib.ox.ac.uk/fsl/fslwiki/PALM). Five thousand sign-flips were performed (Winkler et al., 2014). For the p-value below 0.01, we fit a generalized Pareto distribution to model the tail of the permutation distribution, aiming to improve the precision of the p-values (Knijnenburg et al., 2009; Winkler et al., 2016).

In most cases, we controlled the family-wise error rate using a conventional cluster-forming threshold (i.e., vertex-wise $p < 0.001$, cluster-level FWE corrected $p < 0.05$). In the cases when the cluster-forming threshold was not suitable (i.e., distributed clusters spliced together), we controlled the family-wise error rate using a more conservative vertex-wise threshold (i.e., vertex-wise FWE corrected $p < 0.005$). We corrected the multiple comparisons of the two hemispheres using Bonferroni correction—the threshold set on each hemisphere was vertex-wise $p < 0.001$, cluster-level FWE corrected $p < 0.025$, or vertex-wise FWE corrected $p < 0.0025$.

Brain visualization

The brain results were illustrated using the Connectome Workbench 1.5.0 (https://www.humanconnectome.org/software/connectome-workbench). We mapped the significant brain areas from the fsaverage5 surface to the fsLR surface using the ADAP_BARY_AREA method for visualization purposes. They were displayed on an inflated surface against the group-averaged all sulcus image of 1096 young adults from the dataset of the Human Connectome Project (https://balsa.wustl.edu/reference/pkXDZ).

Acknowledgments

We are thankful to our blind participants. We also thank the Unioni Ciechi of Trento, Mantova, Genova, Savona, Cuneo, Torino, Trieste, Milano and the Institute of the Blind in Milan for helping with the recruitment. We are grateful to Jorge Jovicich for technical assistance in developing fMRI acquisition sequences, Edoardo Camponeschi for recording the stimuli, and Anna D'Urso for her help in data collection.

989 **References**

990 Amedi, A., Jacobson, G., Hendler, T., Malach, R., & Zohary, E. (2002). Convergence of visual and
991 tactile shape processing in the human lateral occipital complex. *Cerebral Cortex*, *12*(11), 1202-
992 1212.

993 Amedi, A., Malach, R., Hendler, T., Peled, S., & Zohary, E. (2001). Visuo-haptic object-related
994 activation in the ventral visual pathway. *Nature Neuroscience*, *4*(3), 324-330.

995 Amedi, A., Raz, N., Azulay, H., Malach, R., & Zohary, E. (2010). Cortical activity during tactile
996 exploration of objects in blind and sighted humans. *Restorative Neurology and Neuroscience*,
997 *28*(2), 143-156.

998 Amedi, A., von Kriegstein, K., van Atteveldt, N. M., Beauchamp, M. S., & Naumer, M. J. (2005).
999 Functional imaging of human crossmodal identification and object recognition. Experimental
000 *Brain Research*, 166(3), 559-571.

001 Bar, M., & Aminoff, E. (2003). Cortical analysis of visual context. *Neuron*, *38*(2), 347-358.

002 Barsalou, L. W., Simmons, W. K., Barbey, A. K., & Wilson, C. D. (2003). Grounding conceptual
003 knowledge in modality-specific systems. *Trends in Cognitive Sciences*, 7(2), 84-91.

004 Battal, C., Gurtubay-Antolin, A., Rezk, M., Mattioni, S., Bertonati, G., Occelli, V., ... & Collignon, O.
005 (2022). Structural and functional network-level reorganization in the coding of auditory motion
006 directions and sound source locations in the absence of vision. *Journal of Neuroscience*, 42(23),
007 4652-4668.

008 Bedny, M. (2017). Evidence from blindness for a cognitively pluripotent cortex. *Trends in Cognitive*
009 *Sciences*, *21*(9), 637-648.

010 Bedny, M., Pascual-Leone, A., Dodell-Feder, D., Fedorenko, E., & Saxe, R. (2011). Language
011 processing in the occipital cortex of congenitally blind adults. *Proceedings of the National*
012 *Academy of Sciences*, *108*(11), 4429-4434.

013 Bi, Y. (2021). Dual coding of knowledge in the human brain. *Trends in Cognitive Sciences,* 25(10),
014 883-895.
015 Bi, Y., Wang, X., & Caramazza, A. (2016). Object domain and modality in the ventral visual
016 pathway. *Trends in Cognitive Sciences,* 20(4), 282-290.
017 Binkofski, F., Kunesch, E., Classen, J., Seitz, R. J., & Freund, H. J. (2001). Tactile apraxia: unimodal
018 apractic disorder of tactile object exploration associated with parietal lobe
019 lesions. *Brain,* 124(1), 132-144.
020 Bloom, P. (1996). Intention, history, and artifact concepts. *Cognition*, *60*(1), 1-29.
021 Bracci, S., & de Beeck, H. O. (2016). Dissociations and associations between shape and category
022 representations in the two visual pathways. *Journal of Neuroscience*, 36(2), 432-444.
023 Bracci, S., & Peelen, M. V. (2013). Body and object effectors: the organization of object
024 representations in high-level visual cortex reflects body–object interactions. *Journal of*
025 *Neuroscience*, 33(46), 18247-18258.
026 Bracci, S., Daniels, N., & Op de Beeck, H. (2017). Task context overrules object-and category-related
027 representational content in the human parietal cortex. *Cerebral Cortex, 27*(1), 310-321.
028 Bridge, H., Thomas, O. M., Minini, L., Cavina-Pratesi, C., Milner, A. D., & Parker, A. J. (2013).
029 Structural and functional changes across the visual cortex of a patient with visual form
030 agnosia. *Journal of Neuroscience*, 33(31), 12779-12791.
031 Buckner, R. L., Andrews-Hanna, J. R., & Schacter, D. L. (2008). The brain's default network: anatomy,
032 function, and relevance to disease. *Annals of the New York Academy of Sciences*, *1124*(1), 1-
033 38.
034 Cant, J. S., & Goodale, M. A. (2007). Attention to form or surface properties modulates different
035 regions of human occipitotemporal cortex. *Cerebral Cortex*, *17*(3), 713-731.

036 Cant, J. S., Arnott, S. R., & Goodale, M. A. (2009). fMR-adaptation reveals separate processing
037 regions for the perception of form and texture in the human ventral stream. *Experimental Brain*
038 *Research*, *192*(3), 391-405.
039 Carlson, T. A., Simmons, R. A., Kriegeskorte, N., & Slevc, L. R. (2014). The emergence of semantic
040 meaning in the ventral temporal pathway. *Journal of Cognitive Neuroscience,* 26(1), 120-131.
041 Castiello, U. (2005). The neuroscience of grasping. *Nature Reviews Neuroscience*, *6*(9), 726-736.
042 Cavina-Pratesi, C., Kentridge, R. W., Heywood, C. A., & Milner, A. D. (2010). Separate channels for
043 processing form, texture, and color: evidence from fMRI adaptation and visual object agnosia.
044 *Cerebral Cortex*, *20*(10), 2319-2332.
045 Chen, J., Snow, J. C., Culham, J. C., & Goodale, M. A. (2018). What role does "elongation" play in
046 "tool-specific" activation and connectivity in the dorsal and ventral visual streams? *Cerebral*
047 *Cortex*, *28*(4), 1117-1131.
048 Coalson, T. S., Van Essen, D. C., & Glasser, M. F. (2018). The impact of traditional neuroimaging
049 methods on the spatial localization of cortical areas. *Proceedings of the National Academy of*
050 *Sciences*, *115*(27), E6356-E6365.
051 Corbetta, M., & Shulman, G. L. (2002). Control of goal-directed and stimulus-driven attention in the
052 brain. *Nature Reviews Neuroscience*, *3*(3), 201-215.
053 Dettmers, C., Liepert, J., Hamzei, F., Binkofski, F., & Weiller, C. (2003). A lesion in the ventrolateral
054 premotor cortex causes difficulties in grasping. *Aktuelle Neurologie*, 30(5), 247-255.
055 Dormal, G., Pelland, M., Rezk, M., Yakobov, E., Lepore, F., & Collignon, O. (2018). Functional
056 preference for object sounds and voices in the brain of early blind and sighted
057 individuals. *Journal of Cognitive Neuroscience*, 30(1), 86-106.
058 Dormal, G., Rezk, M., Yakobov, E., Lepore, F., & Collignon, O. (2016). Auditory motion in the
059 sighted and blind: Early visual deprivation triggers a large-scale imbalance between auditory
060 and “visual” brain regions. *Neuroimage*, 134, 630-644.

061 Dosenbach, N. U., Fair, D. A., Cohen, A. L., Schlaggar, B. L., & Petersen, S. E. (2008). A dual-
062 networks architecture of top-down control. *Trends in Cognitive Sciences*, *12*(3), 99-105.
063 Esteban, O., Markiewicz, C. J., Blair, R. W., Moodie, C. A., Isik, A. I., Erramuzpe, A., ... &
064 Gorgolewski, K. J. (2019). fMRIPrep: a robust preprocessing pipeline for functional MRI.
065 *Nature Methods*, *16*(1), 111-116.
066 Fedorenko, E., Behr, M. K., & Kanwisher, N. (2011). Functional specificity for high-level linguistic
067 processing in the human brain. *Proceedings of the National Academy of Sciences*, *108*(39),
068 16428-16433.
069 Friederici, A. D. (2011). The brain basis of language processing: from structure to function.
070 *Physiological Reviews*, *91*(4), 1357-1392.
071 Friston, K. J., Williams, S., Howard, R., Frackowiak, R. S., & Turner, R. (1996). Movement-related
072 effects in fMRI time-series. *Magnetic Resonance in Medicine, 35*(3), 346-355.
073 Gorgolewski, K., Burns, C. D., Madison, C., Clark, D., Halchenko, Y. O., Waskom, M. L., & Ghosh,
074 S. S. (2011). Nipype: a flexible, lightweight and extensible neuroimaging data processing
075 framework in python. *Frontiers in Neuroinformatics*, *5*, 13.
076 Graves, W. W., Purcell, J., Rothlein, D., Bolger, D. J., Rosenberg-Lee, M., & Staples, R. (2022).
077 Correspondence between cognitive and neural representations for phonology, orthography, and
078 semantics in supramarginal compared to angular gyrus. *Brain Structure and Function*, 1-17.
079 Grill-Spector, K., Kourtzi, Z., & Kanwisher, N. (2001). The lateral occipital complex and its role in
080 object recognition. *Vision Research*, *41*(10-11), 1409-1422.
081 Grinband, J., Wager, T. D., Lindquist, M., Ferrera, V. P., & Hirsch, J. (2008). Detection of time-
082 varying signals in event-related fMRI designs. *Neuroimage*, *43*(3), 509-520.
083 Gurtubay-Antolin, A., Battal, C., Maffei, C., Rezk, M., Mattioni, S., Jovicich, J., & Collignon, O.
084 (2021). Direct structural connections between auditory and visual motion-selective regions in
085 humans. *Journal of Neuroscience*, 41(11), 2393-2405.

086 Hauk, O. (2016). Only time will tell–why temporal information is essential for our neuroscientific
087 understanding of semantics. *Psychonomic Bulletin & Review*, *23*(4), 1072-1079.
088 He, C., Peelen, M. V., Han, Z., Lin, N., Caramazza, A., & Bi, Y. (2013). Selectivity for large
089 nonmanipulable objects in scene-selective visual cortex does not require visual experience.
090 *Neuroimage*, *79*, 1-9.
091 Hömke, L., Amunts, K., Bönig, L., Fretz, C., Binkofski, F., Zilles, K., & Weder, B. (2009). Analysis
092 of lesions in patients with unilateral tactile agnosia using cytoarchitectonic probabilistic maps.
093 *Human Brain Mapping*, *30*(5), 1444-1456.
094 Humphreys, G. F., Ralph, M. A. L., & Simons, J. S. (2021). A unifying account of angular gyrus
095 contributions to episodic and semantic cognition. *Trends in Neurosciences*, 44(6), 452-463.
096 James, T. W., Culham, J., Humphrey, G. K., Milner, A. D., & Goodale, M. A. (2003). Ventral occipital
097 lesions impair object recognition but not object-directed grasping: an fMRI study. *Brain*,
098 *126*(11), 2463-2475.
099 James, T. W., James, K. H., Humphrey, G. K., & Goodale, M. A. (2006). Do visual and tactile object
100 representations share the same neural substrate. *Touch and blindness: Psychology and*
101 *neuroscience*, 139-155.
102 Jeannerod, M., Arbib, M. A., Rizzolatti, G., & Sakata, H. (1995). Grasping objects: the cortical
103 mechanisms of visuomotor transformation. *Trends in Neurosciences*, *18*(7), 314-320.
104 Kalénine, S., & Buxbaum, L. J. (2016). Thematic knowledge, artifact concepts, and the left posterior
105 temporal lobe: Where action and object semantics converge. *Cortex*, 82, 164-178.
106 Kanjlia, S., Lane, C., Feigenson, L., & Bedny, M. (2016). Absence of visual experience modifies the
107 neural basis of numerical thinking. *Proceedings of the National Academy of Sciences*, *113*(40),
108 11172-11177.
109 Klein, A., & Tourville, J. (2012). 101 labeled brain images and a consistent human cortical labeling
110 protocol. *Frontiers in Neuroscience*, *6*, 171.

Knijnenburg, T. A., Wessels, L. F., Reinders, M. J., & Shmulevich, I. (2009). Fewer permutations, more accurate P-values. *Bioinformatics, 25*(12), i161-i168.

Konkle, T., & Oliva, A. (2012). A real-world size organization of object responses in occipitotemporal cortex. *Neuron*, *74*(6), 1114-1124.

Koo, T. K., & Li, M. Y. (2016). A guideline of selecting and reporting intraclass correlation coefficients for reliability research. *Journal of Chiropractic Medicine*, *15*(2), 155-163.

Kriegeskorte, N., & Mur, M. (2012). Inverse MDS: Inferring dissimilarity structure from multiple item arrangements. *Frontiers in Psychology*, *3*, 245.

Kriegeskorte, N., Goebel, R., & Bandettini, P. (2006). Information-based functional brain mapping. *Proceedings of the National Academy of Sciences*, *103*(10), 3863-3868.

Kriegeskorte, N., Mur, M., & Bandettini, P. A. (2008). Representational similarity analysis-connecting the branches of systems neuroscience. *Frontiers in Systems Neuroscience*, *2*, 4.

Kveraga, K., Ghuman, A. S., Kassam, K. S., Aminoff, E. A., Hämäläinen, M. S., Chaumon, M., & Bar, M. (2011). Early onset of neural synchronization in the contextual associations network. *Proceedings of the National Academy of Sciences*, *108*(8), 3389-3394.

Lacey, S., Tal, N., Amedi, A., & Sathian, K. (2009). A putative model of multisensory object representation. *Brain Topography*, *21*(3), 269-274.

Lane, C., Kanjlia, S., Omaki, A., & Bedny, M. (2015). "Visual" cortex of congenitally blind adults responds to syntactic movement. *Journal of Neuroscience*, *35*(37), 12859-12868.

Lane, C., Kanjlia, S., Richardson, H., Fulton, A., Omaki, A., & Bedny, M. (2017). Reduced left lateralization of language in congenitally blind individuals. *Journal of Cognitive Neuroscience*, *29*(1), 65-78.

Lederman, S. J., Klatzky, R. L., Chataway, C., & Summers, C. D. (1990). Visual mediation and the haptic recognition of two-dimensional pictures of common objects. *Perception & Psychophysics*, *47*(1), 54-64.

136 Lee Masson, H., Bulthé, J., Op de Beeck, H. P., & Wallraven, C. (2016). Visual and haptic shape
137 processing in the human brain: unisensory processing, multisensory convergence, and top-
138 down influences. *Cerebral Cortex*, *26*(8), 3402-3412.
139 Lloyd, S. (1982). Least squares quantization in PCM. *IEEE Transactions on Information Theory*, *28*(2),
140 129-137.
141 Martin, A. (2016). GRAPES—Grounding representations in action, perception, and emotion systems:
142 How object properties and categories are represented in the human brain. *Psychonomic Bulletin*
143 *& Review*, 23(4), 979-990.
144 Martin, C. B., Douglas, D., Newsome, R. N., Man, L. L., & Barense, M. D. (2018). Integrative and
145 distinctive coding of visual and conceptual object features in the ventral visual stream. *Elife*, *7*,
146 e31873.
147 Martin, M., Beume, L., Kümmerer, D., Schmidt, C. S., Bormann, T., Dressing, A., ... & Weiller, C.
148 (2016). Differential roles of ventral and dorsal streams for conceptual and production-related
149 components of tool use in acute stroke patients. *Cerebral Cortex,* 26(9), 3754-3771.
150 Mattioni, S., Rezk, M., Battal, C., Bottini, R., Mendoza, K. E. C., Oosterhof, N. N., & Collignon, O.
151 (2020). Categorical representation from sound and sight in the ventral occipito-temporal cortex
152 of sighted and blind. *Elife*, 9.
153 McGraw, K. O., & Wong, S. P. (1996). Forming inferences about some intraclass correlation
154 coefficients. *Psychological Methods*, *1*(1), 30.
155 Miceli, G., Fouch, E., Capasso, R., Shelton, J. R., Tomaiuolo, F., & Caramazza, A. (2001). The
156 dissociation of color from form and function knowledge. *Nature neuroscience*, 4(6), 662-667.
157 Milner, A. D., Perrett, D. I., Johnston, R. S., Benson, P. J., Jordan, T. R., Heeley, D. W., ... & Davidson,
158 D. L. W. (1991). Perception and action in 'visual form agnosia.' *Brain*, *114*(1), 405-428.
159 Mirman, D., Landrigan, J. F., & Britt, A. E. (2017). Taxonomic and thematic semantic systems.
160 *Psychological Bulletin*, *143*(5), 499.

161 Misaki, M., Kim, Y., Bandettini, P. A., & Kriegeskorte, N. (2010). Comparison of multivariate
162 classifiers and response normalizations for pattern-information fMRI. *Neuroimage*, *53*(1), 103-
163 118.
164 Mumford, J. A., Poline, J. B., & Poldrack, R. A. (2015). Orthogonalization of regressors in fMRI
165 models. *PloS one*, *10*(4), e0126255.
166 Murata, A., Fadiga, L., Fogassi, L., Gallese, V., Raos, V., & Rizzolatti, G. (1997). Object
167 representation in the ventral premotor cortex (area F5) of the monkey. *Journal of*
168 *Neurophysiology*, 78(4), 2226-2230.
169 Murata, A., Gallese, V., Luppino, G., Kaseda, M., & Sakata, H. (2000). Selectivity for the shape, size,
170 and orientation of objects for grasping in neurons of monkey parietal area AIP. *Journal of*
171 *Neurophysiology*, 83(5), 2580-2601.
172 Noppeney, U., Friston, K. J., & Price, C. J. (2003). Effects of visual deprivation on the organization
173 of the semantic system. *Brain*, 126(7), 1620-1627.
174 Paivio, A. (1986). Mental Representation: A Dual-Coding Approach. *New York: Oxford University*
175 *Press*.
176 Pascual-Leone, A., & Hamilton, R. (2001). The metamodal organization of the brain. *Progress in*
177 *Brain Research*, *134*, 427-445.
178 Peelen, M. V., Bracci, S., Lu, X., He, C., Caramazza, A., & Bi, Y. (2013). Tool selectivity in left
179 occipitotemporal cortex develops without vision. *Journal of cognitive neuroscience*, 25(8),
180 1225-1234.
181 Peelen, M. V., He, C., Han, Z., Caramazza, A., & Bi, Y. (2014). Nonvisual and visual object shape
182 representations in occipitotemporal cortex: evidence from congenitally blind and sighted adults.
183 *Journal of Neuroscience*, *34*(1), 163-170.

Peuskens, H., Claeys, K. G., Todd, J. T., Norman, J. F., Van Hecke, P., & Orban, G. A. (2004). Attention to 3-D shape, 3-D motion, and texture in 3-D structure from motion displays. *Journal of Cognitive Neuroscience*, *16*(4), 665-682.

Pietrini, P., Furey, M. L., Ricciardi, E., Gobbini, M. I., Wu, W. H. C., Cohen, L., ... & Haxby, J. V. (2004). Beyond sensory images: Object-based representation in the human ventral pathway. *Proceedings of the National Academy of Sciences,* 101(15), 5658-5663.

Poirier, C., Collignon, O., Scheiber, C., Renier, L., Vanlierde, A., Tranduy, D., ... & De Volder, A. G. (2006). Auditory motion perception activates visual motion areas in early blind subjects. *Neuroimage*, *31*(1), 279-285.

Popham, S. F., Huth, A. G., Bilenko, N. Y., Deniz, F., Gao, J. S., Nunez-Elizalde, A. O., & Gallant, J. L. (2021). Visual and linguistic semantic representations are aligned at the border of human visual cortex. *Nature Neuroscience*, 24(11), 1628-1636.

Power, J. D., Barnes, K. A., Snyder, A. Z., Schlaggar, B. L., & Petersen, S. E. (2012). Spurious but systematic correlations in functional connectivity MRI networks arise from subject motion. *Neuroimage*, *59*(3), 2142-2154.

Ptito, M., Matteau, I., Gjedde, A., & Kupers, R. (2009). Recruitment of the middle temporal area by tactile motion in congenital blindness. *Neuroreport*, *20*(6), 543-547.

Ricciardi, E., Bonino, D., Pellegrini, S., & Pietrini, P. (2014). Mind the blind brain to understand the sighted one! Is there a supramodal cortical functional architecture? *Neuroscience & Biobehavioral Reviews*, *41*, 64-77.

Ricciardi, E., Vanello, N., Sani, L., Gentili, C., Scilingo, E. P., Landini, L., ... & Pietrini, P. (2007). The effect of visual experience on the development of functional architecture in hMT+. *Cerebral Cortex*, *17*(12), 2933-2939.

Rousseeuw, P. J. (1987). Silhouettes: a graphical aid to the interpretation and validation of cluster analysis. *Journal of Computational and Applied Mathematics*, *20*, 53-65.

209 Seeley, W. W., Menon, V., Schatzberg, A. F., Keller, J., Glover, G. H., Kenna, H., ... & Greicius, M.
210 D. (2007). Dissociable intrinsic connectivity networks for salience processing and executive
211 control. *Journal of Neuroscience*, *27*(9), 2349-2356.
212 Simmons, W. K., Ramjee, V., Beauchamp, M. S., McRae, K., Martin, A., & Barsalou, L. W. (2007).
213 A common neural substrate for perceiving and knowing about color. *Neuropsychologia*, 45(12),
214 2802-2810.
215 Snow, J. C., Goodale, M. A., & Culham, J. C. (2015). Preserved haptic shape processing after bilateral
216 LOC lesions. *Journal of Neuroscience*, 35(40), 13745-13760.
217 Stilla, R., & Sathian, K. (2008). Selective visuo-haptic processing of shape and texture. *Human Brain*
218 *Mapping*, *29*(10), 1123-1138.
219 Striem-Amit, E., Wang, X., Bi, Y., & Caramazza, A. (2018). Neural representation of visual concepts
220 in people born blind. *Nature Communications*, *9*(1), 1-12.
221 Tal, N., & Amedi, A. (2009). Multisensory visual–tactile object related network in humans: insights
222 gained using a novel crossmodal adaptation approach. *Experimental Brain Research*, *198*(2),
223 165-182.
224 Thompson-Schill, S. L. (2003). Neuroimaging studies of semantic memory: inferring "how" from
225 "where". *Neuropsychologia,* 41(3), 280-292.
226 Van Ackeren, M. J., Barbero, F. M., Mattioni, S., Bottini, R., & Collignon, O. (2018). Neuronal
227 populations in the occipital cortex of the blind synchronize to the temporal dynamics of
228 speech. *ELife*, *7*.
229 Vassilvitskii, S., & Arthur, D. (2006). k-means++: The advantages of careful seeding. In *Proceedings*
230 *of the Eighteenth Annual ACM-SIAM Symposium on Discrete Algorithms*.
231 Vernon, R. J., Gouws, A. D., Lawrence, S. J., Wade, A. R., & Morland, A. B. (2016). Multivariate
232 patterns in the human object-processing pathway reveal a shift from retinotopic to shape

curvature representations in lateral occipital areas, LO-1 and LO-2. *Journal of Neuroscience*, *36*(21), 5763-5774.

Wang, X., Peelen, M. V., Han, Z., He, C., Caramazza, A., & Bi, Y. (2015). How visual is the visual cortex? Comparing connectional and functional fingerprints between congenitally blind and sighted individuals. *Journal of Neuroscience,* 35(36), 12545-12559.

Winkler, A. M., Ridgway, G. R., Douaud, G., Nichols, T. E., & Smith, S. M. (2016). Faster permutation inference in brain imaging. *Neuroimage, 141,* 502-516.

Winkler, A. M., Ridgway, G. R., Webster, M. A., Smith, S. M., & Nichols, T. E. (2014). Permutation inference for the general linear model. *Neuroimage, 92,* 381-397.

Xu, Y., He, Y., & Bi, Y. (2017). A tri-network model of human semantic processing. *Frontiers in Psychology*, *8*, 1538.

Xu, Y., Lin, Q., Han, Z., He, Y., & Bi, Y. (2016). Intrinsic functional network architecture of human semantic processing: modules and hubs. *Neuroimage*, *132*, 542-555.

Xu, Y., Wang, X., Wang, X., Men, W., Gao, J. H., & Bi, Y. (2018). Doctor, teacher, and stethoscope: neural representation of different types of semantic relations. *Journal of Neuroscience*, *38*(13), 3303-3317.

Zhang, M., Weisser, V. D., Stilla, R., Prather, S. C., & Sathian, K. (2004). Multisensory cortical processing of object shape and its relation to mental imagery. *Cognitive, Affective, & Behavioral Neuroscience*, *4*(2), 251-259.

Zuo, X. N., Xu, T., Jiang, L., Yang, Z., Cao, X. Y., He, Y., ... & Milham, M. P. (2013). Toward reliable characterization of functional homogeneity in the human brain: preprocessing, scan duration, imaging resolution and computational space. *Neuroimage*, *65*, 374-386.

Table 1. Accuracy and reaction time during fMRI scanning

	Accuracy (%, M ± SD)		Reaction Time (ms, M ± SD) *	
	Shape Task	Conceptual Task	Shape Task	Conceptual Task
EB (N = 16)	95.0 ± 4.1	96.9 ± 1.6	1798 ± 313	1590 ± 234
SC (N = 16)	97.4 ± 2.7	98.1 ± 1.3	1689 ± 265	1546 ± 221
IS (N = 16)	95.9 ± 2.9	97.7 ± 1.5	1999 ± 345	1866 ± 376

* Mean reaction time across all the correct trials within each participant

Table 2. Neural representation in bilateral ILOTC

Three-way Mixed ANOVA *	**Left ILOTC**		**Right ILOTC**	
Groups (EB vs. SC)	F(1, 30) = 1.809	p = 0.189	F(1, 30) = 0.466	p = 0.500
Tasks (Shape vs. Conceptual)	F(1, 30) = 2.829	p = 0.103	F(1, 30) = 0.025	p = 0.874
Representations (Shape vs. Conceptual)	**F(1, 30) = 21.814**	**p < 0.001**	**F(1, 30) = 11.871**	**p = 0.002**
Groups × Tasks	F(1, 30) = 2.047	p = 0.163	F(1, 30) = 0.157	p = 0.695
Groups × Representations	F(1, 30) = 2.056	p = 0.162	F(1, 30) = 0.055	p = 0.816
Tasks × Representations	**F(1, 30) = 15.596**	**p < 0.001**	**F(1, 30) = 10.116**	**p = 0.003**
Groups × Tasks × Representations	F(1, 30) = 0.097	p = 0.757	F(1, 30) = 0.066	p = 0.799

* The Groups factor was between-subject, whereas Tasks and Representations were within-subject factors.

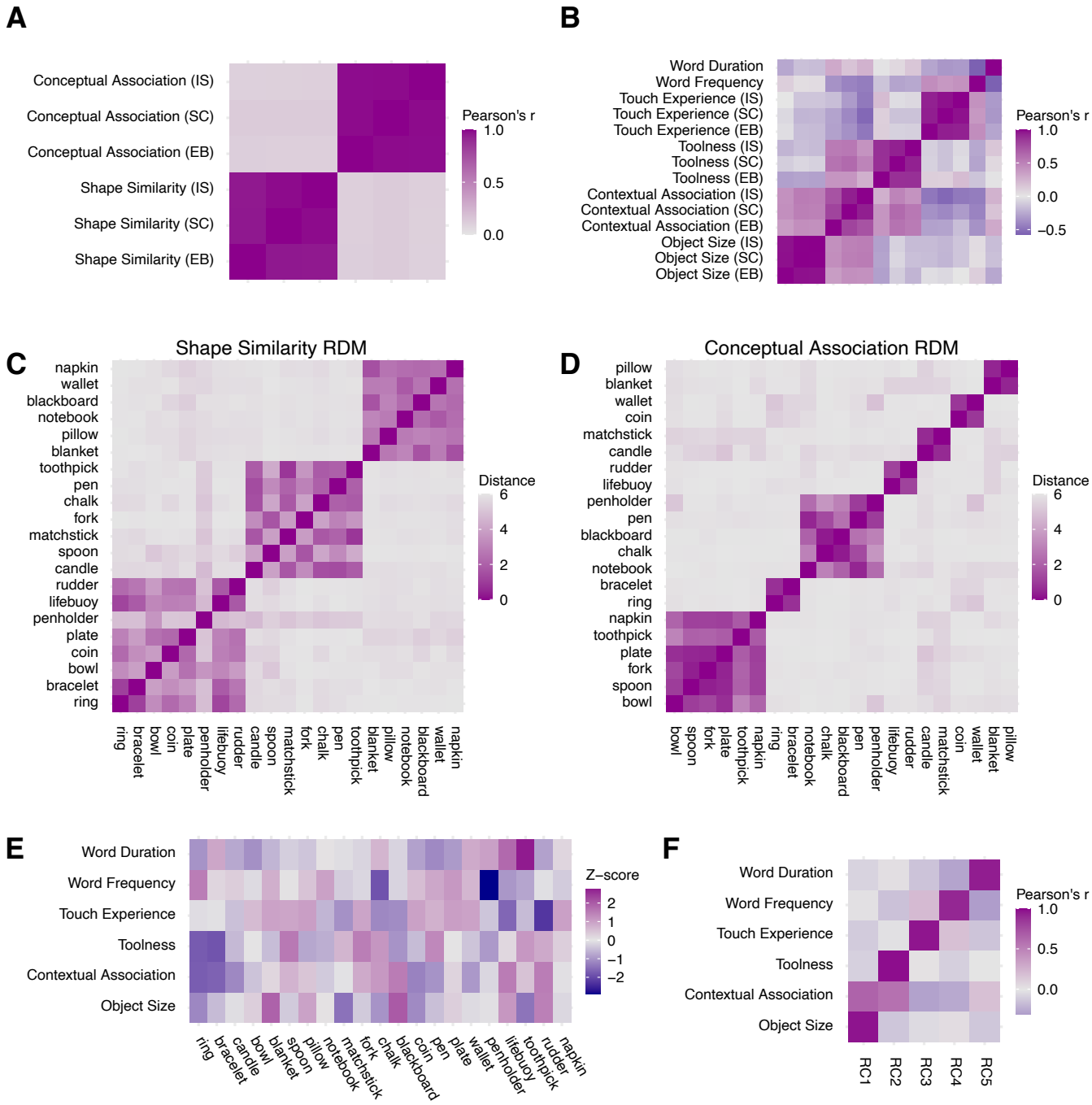

Figure 1. Stimulus information. (A) Correlation between ratings on pairwise shape similarity and pairwise conceptual association across three participant groups. (B) Correlation among linguistic variables and ratings on other object properties across three participant groups. (C) Pairwise ratings on shape similarity (i.e., the Shape Similarity RDM). (D) Pairwise ratings on conceptual association (the Conceptual Association RDM). (E) Linguistic variables and ratings on other object properties. (F) Correlations between the first five rotated components (RC) and linguistic variables and ratings on other object properties.

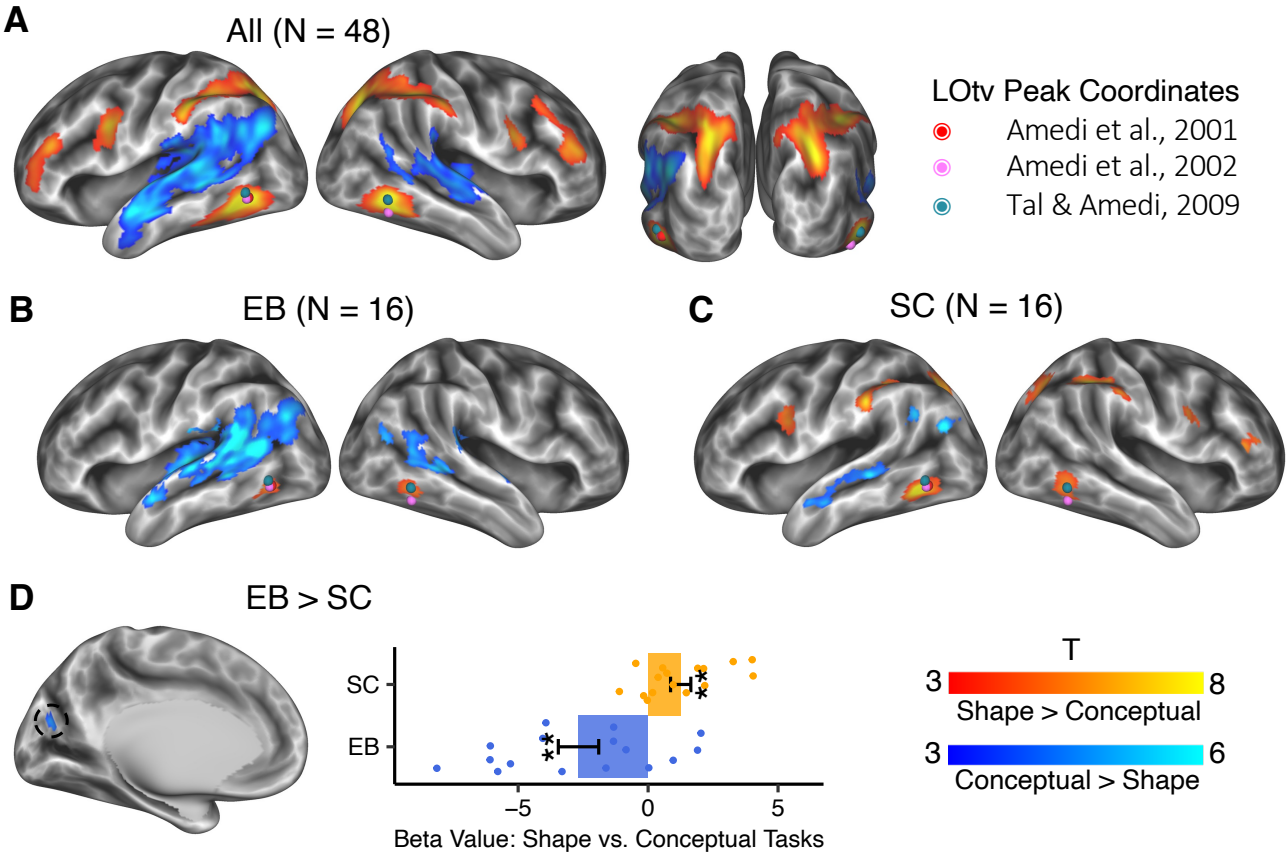

Figure 2. Specific brain activation in shape and conceptual tasks (vertex-wise $p < 0.001$, cluster-level FWE corrected $p < 0.05$). Dots in colors denote the location of LOtv in three representative studies. (A) Shape versus conceptual tasks across all the participants. (B) Shape versus conceptual tasks in EB. (C) Shape versus conceptual tasks in SC. (D) Interaction between Groups (EB vs. SC) and Tasks (Shape vs. Conceptual). The error bars indicate the standard error. **: $p < 0.01$.

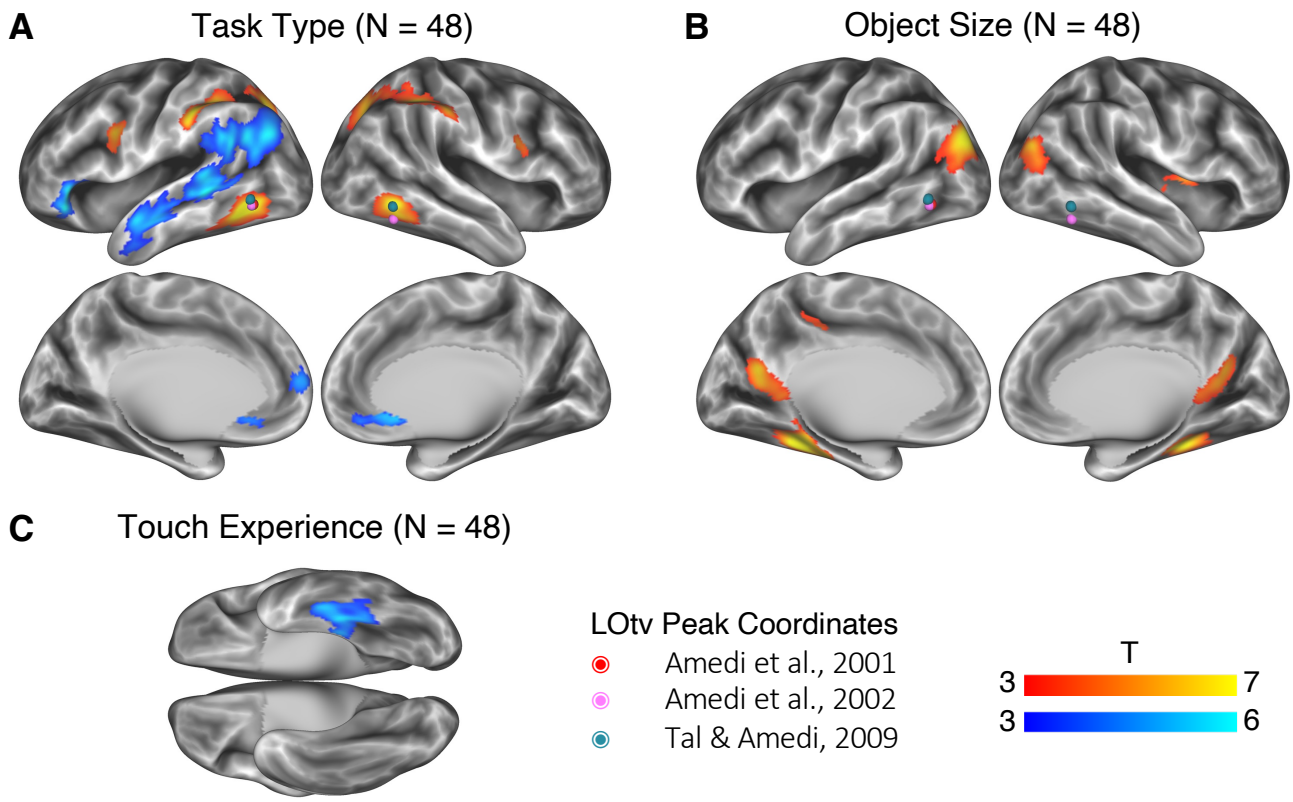

Figure 3. Neural correlates of task types and other object properties (vertex-wise $p < 0.001$, cluster-level FWE corrected $p < 0.05$). Dots in colors denote the location of LOtv in three representative studies. (A) Neural correlates of task types (the shape task coded as 1 and the conceptual task coded as -1). (B) Neural correlates of object size. Activations in the significant brain areas positively correlated with object size, i.e., larger objects induced higher activation. (C) Neural correlates of touch experience. Activations in the significant brain area negatively correlated with touch experience, i.e., less-touched objects induced higher activation.

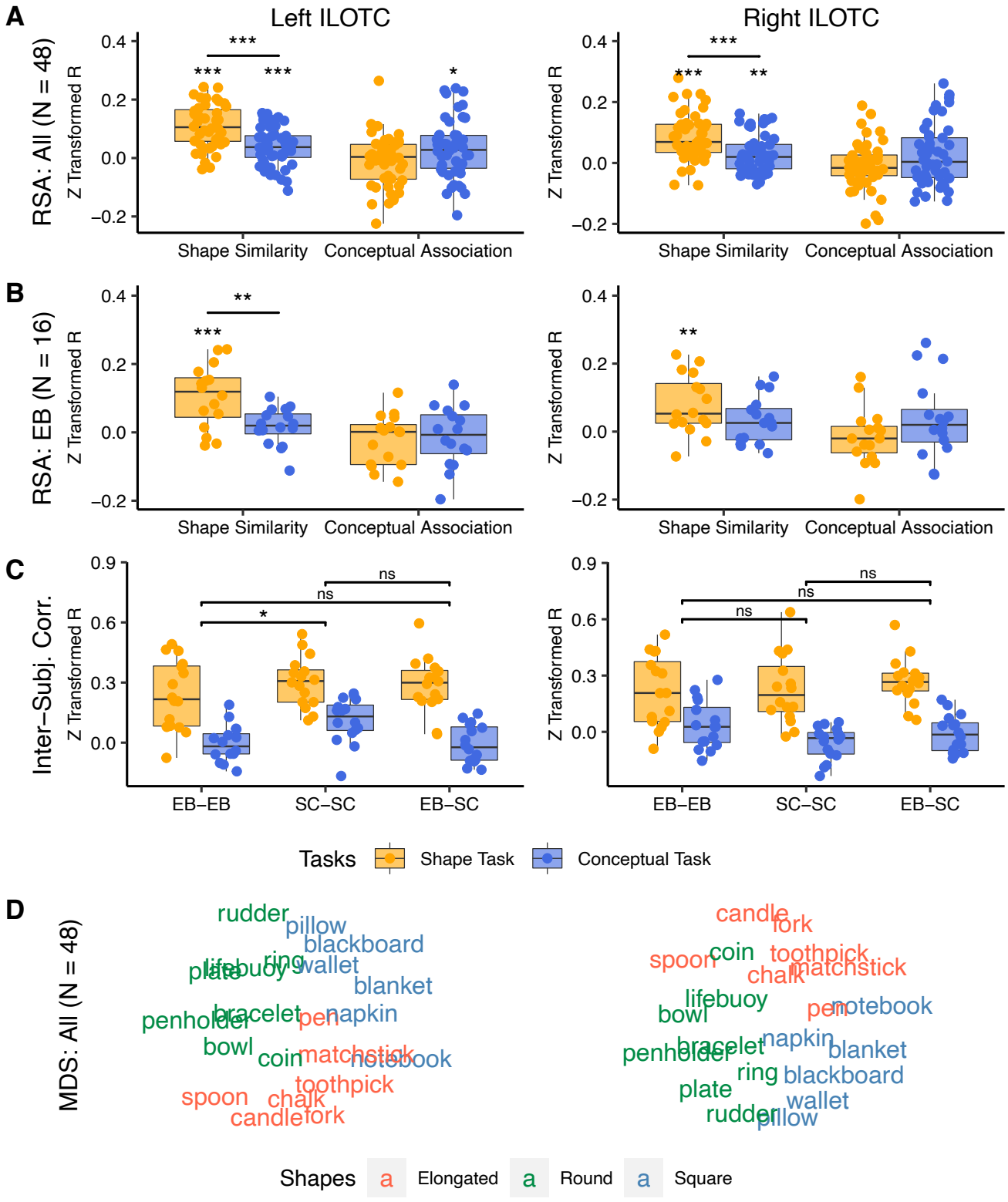

Figure 4. Neural representations of bilateral ILOTC. The left column showed the neural representation in the left ILOTC. The right column showed the neural representation of the right ILOTC. (A) The RSA results across all participants (N = 48). (B) The RSA results in EB (N = 16). (C) Inter-subject correlation between brain RDMs within and between EB and SC groups. (D) The MDS visualization of the mean brain RDM of the ILOTC across all participants (N = 48). ns: not significant, *: $p < 0.05$, **: $p < 0.01$, ***: $p < 0.001$.

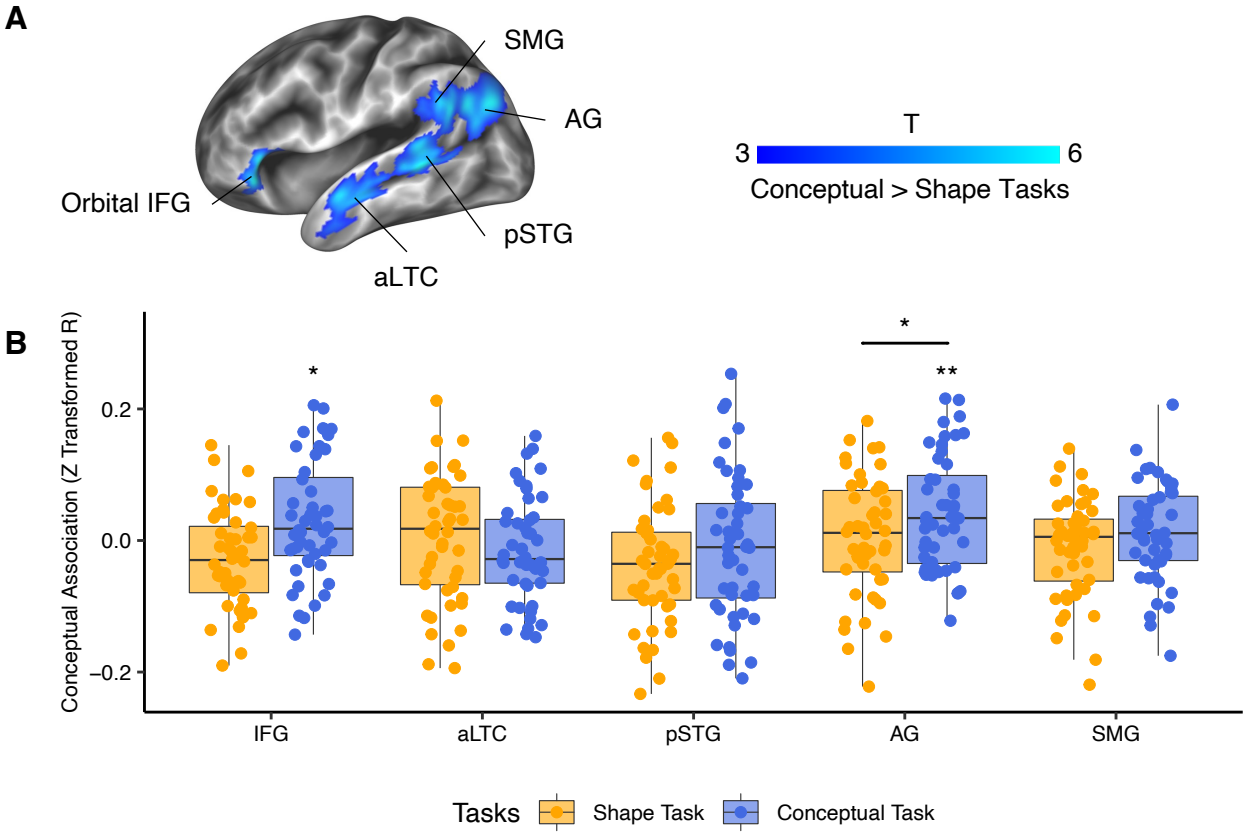

Figure 5. RSA results of conceptual association in the brain areas with greater activation in the conceptual task than in the shape task. (A) Brain areas with significantly greater activation in the conceptual task than in the shape task defined in Figure 2A. (B) RSA results of these conceptual-relevant areas in shape and conceptual tasks. *: $p < 0.05$, **: $p < 0.01$.

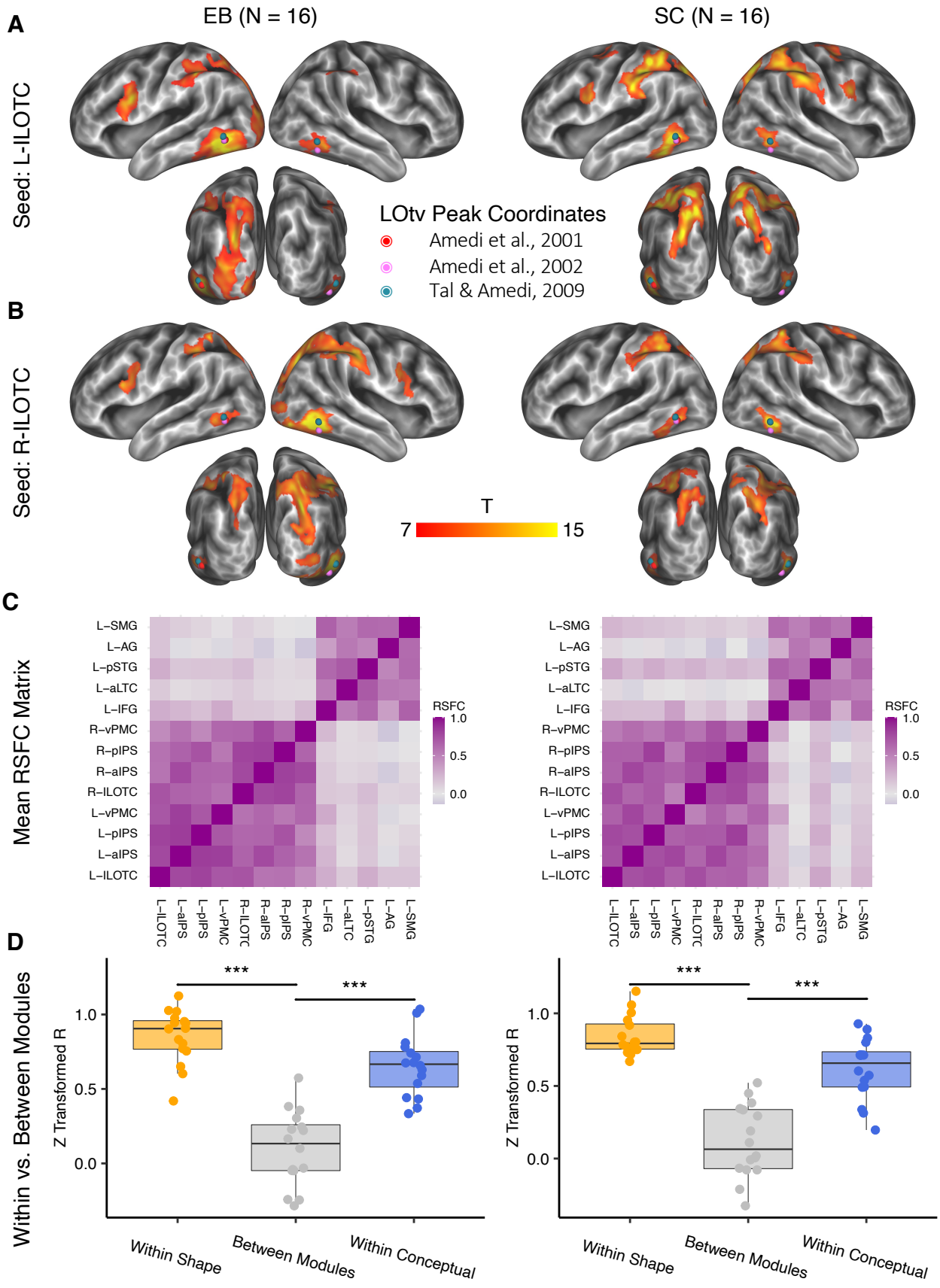

Figure 6. Shape and conceptual brain network. The left panel shows the RSFC results in EB, and the right panel shows the RSFC results in SC. (A, B) the significant seed-based RSFC results in the left

ILOTC (A) and the right ILOTC (B) (vertex-wise FWE corrected $p < 0.005$, cluster size > 400 mm2). Dots in colors denote the location of LOtv in three representative studies. (C) the mean RSFC matrix across participants in EB and SC among the shape- and conceptual-relevant brain areas. (D) Comparison among the mean RSFC among the shape-relevant regions ("Within Shape"), among the conceptual-relevant regions ("Within Conceptual"), and between the shape- and the conceptual-relevant regions ("Between Modules"). ***: $p < 0.001$.